SYNTHESIS AND CHARACTERIZATION OF IRON OXIDE NANOPARTICLES

By

Saba Naz

(336-FBAS/MS PHY/S15)

DEPARTMENT OF PHYSICS

FACULTY OF BASIC AND APPLIED SCIENCES,

INTERNATIONAL ISLAMIC UNIVERSITY, ISLAMABAD

(2017)

SYNTHESIS AND CHARACTERIZATION OF IRON OXIDE NANOPARTICLES

By

SABA NAZ

(336-FBAS/MS PHY/S15)

Supervisor

Dr. Waqar Adil

Co-Supervisor

Dr. Shamaila Sajjad

DEPARTMENT OF PHYSICS

FACULTY OF BASIC AND APPLIED SCIENCES,

INTERNATIONAL ISLAMIC UNIVERSITY, ISLAMABAD

(2017)

Nanotechnology.

Iron oxide

Green synthesis

X-Ray diffraction.

SYNTHESIS AND CHARACTERIZATION OF IRON OXIDE NANOPARTICLES

By

Saba Naz

(Registration No. 336-FBAS/MS PHY/S15)

A thesis submitted to

Department of Physics

for the award of the degree of

MS Physics (Nanotechnology)

Signature: _____

(Chairperson, Department of Physics)

Dr. Shamaila Sajj
Chairperson
Department of Physics (FC, FBA
International Islamic Universi
Islamabad

Signature: _____

(Dean FBAS, IIUI, Islamabad)

INTERNATIONAL ISLAMIC UNIVERSITY, ISLAMABAD

FACULTY OF BASIC AND APPLIED SCIENCES

DEPARTMENT OF PHYSICS

Dated:14-06-2017

FINAL APPROVAL

It is certified that the work presented in this thesis entitled

"Synthesis and characterization of iron oxide nanoparticles"

by **Ms. Saba Naz** bearing Registration No. **336-FBAS/MS PHY/S15** is of sufficient standard in scope and quality for the award of degree of MS Physics from International Islamic University, Islamabad.

COMMITTEE

External Examiner

Dr. Muhammad Usman
Experimental Physics Laboratories,
National Center of Physics,
Islamabad, Pakistan

Internal Examiner

Dr. Imran Murtaza
Assistant Professor
International Islamic University,
Islamabad

Supervisor

Dr. Waqar Adil Syed
Associate Professor
International Islamic University,
Islamabad

Co-Supervisor

Dr. Shamaila Sajjad
Chairperson, Department of Physics,
Assistant Professor
International Islamic University, Islamabad

Dr. Shamaila Sajjad
Chairperson
Department of Physics (FBAS)
International Islamic University
Islamabad


بسم الله الرحمن الرحيم

A thesis submitted to

Department of Physics

International Islamic University Islamabad

As a partial fulfilment for the award of the degree of

MS in Physics (Nanotechnology)

Declaration

It is hereby declaring that this thesis work, neither as a whole nor a part of it has been copied out from any source. Further, work presented in this dissertation has not been submitted in support of any application for any other degree or qualification to any other university or institute and is considerable under the plagiarism rules of Higher Education Commission (HEC), Pakistan.

Saba Naz

(336-FBAS/MS PHY/S15)

DEDICATED

To

My Parents

Acknowledgement

For the very first, all praises are to **Allah Almighty**, the Most Merciful and Beneficent, who enabled me to complete my project work. And His Holy Prophet Muhammad (SAW), the most Perfect among all ever born on earth, and forever being the light of guidance and knowledge for humanity.

I am very thankful to my Supervisor **Dr. Waqar Adil** for full cooperation and encouragement. I feel great honor to express the deepest sense of appreciation to my respected Co-Supervisor **Dr. Shamaila Sajjad** for her inspiring guidance, encouragement, support and keen interest during the entire work.

Words are lacking to express my deepest feeling to my parents, brothers and sister for their back-up support and prayers and special thanks to all my friends for helping and encouragement attitude. May Allah's special blessing with all of them.

Table of Contents

List of Figures

List of Tables

List of abbreviations

Fe_3O_4	Magnetite
NPs	Nanoparticles
XRD	X-Ray Diffraction
SEM	Scanning Electron Microscopy
FTIR	Fourier Transform Infrared Spectroscopy
UV-Visible	Ultra Violet Visible Spectroscopy
EDX	Energy Dispersive X-Ray
VSM	Vibrating Sample Magnetometer
nm	Nanometre
cm^{-1}	Per centimetre
ev	Electron Volt
VTT	Verwey transition temperature
T_M	Morin transition temperature
T_N	Neel temperature
T_C	Curie temperature

Abstract

This work investigates a facile and low cost technique to synthesize the iron oxide NPs via chemical and green route. Green synthesized iron oxide NPs was achieved by utilizing rich polyphenols in ginger, mint and spinach leaves as a reducing and stabilizing agent. As synthesized nanoparticles were calcined at 300 °C and 500 °C and then studied their properties.

Then these samples were characterized via different techniques like XRD (X-Ray diffraction) for the identification of phase and crystal structure, SEM (scanning electron microscopy) for particle size and surface morphology analysis, FTIR (Fourier transform infrared spectroscopy) for chemical investigation and EDX (energy dispersive X-Ray) spectroscopy for determination of elemental composition.

XRD pattern determined the inverse spinel structure of chemically synthesized nanoparticles which shows that particles are pure magnetite with crystallite size of 17 nm. At 300 °C, only few peaks of hematite showed and the phase transformation more proceeds to hematite at higher temperature about 500 °C. The presence of these two phases also confirmed by FTIR analysis. Octahedral and tetrahedral vibrational bands of inverse spinel structure at 700 cm^{-1} and 490 cm^{-1} corresponds to magnetite (Fe_3O_4) phase. In green synthesized nanoparticles, octahedral and tetrahedral vibrational bands occurred at 485 cm^{-1} and 657 cm^{-1} corresponds to magnetite phase. There are some signatures of the presence of hematite which is manifested by a band at 520 cm^{-1}. SEM analysis showed the spherical and roughly spherical morphology of chemically and green synthesized nanoparticles, with size of less than 100 nm respectively. EDX analysis indicates that prepared sample comprises of iron and oxygen, which confirms the formation of iron oxide.

Chapter No.1

1 Introduction

1.1 Nanotechnology:

Nanotechnology is the manipulation of material or objects on a molecular, atomic and supra-molecular scale. The particles are well-defined as a small thing that perform as the whole unit because of its transportation and properties.

Nanotechnology is the branch of science that deals with the synthesis of nanomaterials, analyse and their innovative properties that is altered from bulk to Nano level. It has so many biomedical applications due to its unique properties, i.e. [1]– [2], catalysis [3], wastewater treatment [4], sensors [5], electronics [6]

The particles between about 1 to 100 nanometers in size are nanoparticles. The nanoparticles are of incredible consideration due to their exceptional properties, for example, mechanical, basic, softening point, Electrical conductivity, Optical, and Magnetic.

A few cases said are the versatile module diminishes significantly with the decline in size to nanoscale and the hardness increments with abatement in size. Likewise, the liquefying point lessens with a diminishing in molecule estimate since dissolving begins from the surface and with size decrease the surface to mass particle proportion increments. Electrical conductivity lessens as the resistivity increments. Nanoparticle can be synthesized in two different ways.

1.1.1 Bottom-Up Technique:

In this technique, atoms and molecules are arranged to form the nanomaterials of the desired size and shape by controlling reaction constraints.

1.1.2 Top-Down Technique:

In this technique, molecules and the atoms are removed from the bulk level to acquire desired shape nanoparticles.

Nanoparticles can be synthesized by these two techniques, such as metal oxide nanoparticles, Non-metallic nanoparticles, bimetallic nanoparticles etc. Metallic nanoparticles have extraordinary intrigue since it demonstrates Surface Plasmon Resonance Phenomenon [7].

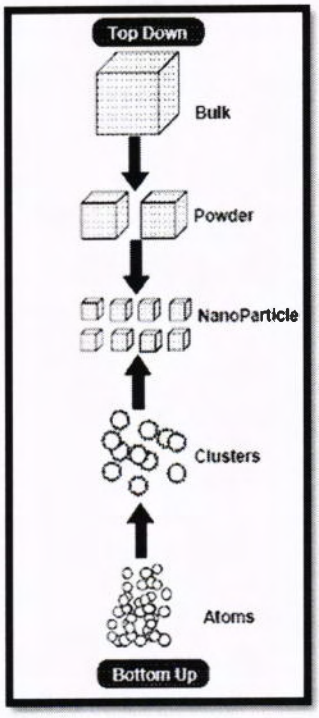

Figure 1.1: Top-down and bottom-up approaches for the synthesis of nanoparticles

The metallic nanoparticles can be isolated into Noble metals (gold, platinum, palladium and silver) which are more steady and the other sort are Magnetic nanoparticles (Iron, Nickel, and Cobalt) these are for the most part ferromagnetic materials. In magnetic nanomaterials, iron has an excessive interest because it is modest, effortlessly accessible and shows more attractive properties than other metallic components. The iron nanoparticles mainly exist in the form of iron oxide because iron nanoparticles are not stable in the atmosphere that is why it gets changed to iron oxide very quickly.

1.2 Introduction to iron oxide:

Iron is a Block D, Period 4 element, while oxygen is a Block P, Period 2 element. Iron is 4th most common element in the earth's crust and atomic number is 26. It is a metal in first transition series. Forming much of earth's outer and inner core. Most common form of iron is iron oxide.

There are sixteen known forms of iron oxides which are found as oxides and oxyhydroxides [8];

Iron Oxides:

There are three main forms of iron oxides:

- Iron (II) oxide, (FeO)
- Iron (II, III) oxide, (Fe_3O_4)
- Iron (III) oxide, (Fe_2O_3)

Iron (III) oxide has four different phases:

- ➢ α-Fe_2O_3
- ➢ β-Fe_2O_3
- ➢ γ-Fe_2O_3
- ➢ ε-Fe_2O_3

Iron Oxide-hydroxide:

- α -FeOOH
- β -FeOOH
- γ-FeOOH
- δ-FeOOH
- $Fe_5HO_8 \cdot 4H_2O$
- FeOOH
- $Fe_8O_8(OH)_6(SO) \cdot nH_2O$

Iron hydroxide

- $Fe(OH)_2$
- $Fe(OH)_3$

All these forms of iron oxides are changed because of lattice structure

1.2.1 Iron (ll) oxide or wustite (FeO):

Iron(II) oxide (FeO) is an inorganic compound having formula FeO, which is rare. The mineral form of FeO is recognised as wüstite. It exists as a black coloured powder, that is in some cases mistook for rust, which comprises of hydrated iron(III) oxide (ferric oxide). Iron(II) oxide also discusses to a class of associated non-stoichiometric compounds having composition range from $Fe_{0.84}O$ to $Fe_{0.95}O$, which are iron deficient [9].

1.2.1.1 Structure of wustite:

The wüstite has the cubic unit cell in which each iron ion is bounded by the six oxygen atoms. The bond length between iron and oxygen atoms is 2.16 Armstrong.

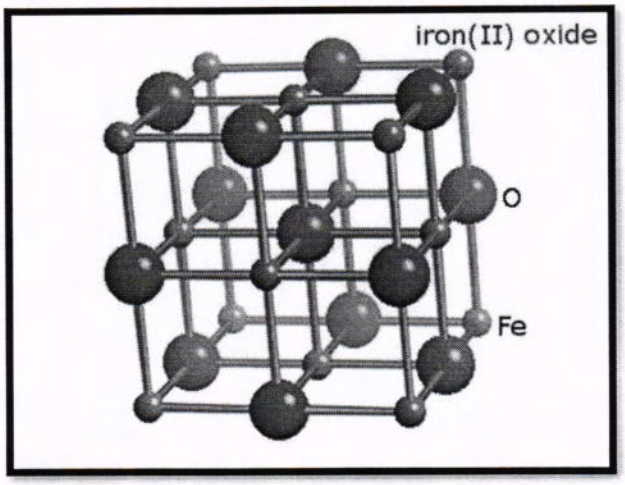

Figure 1.2: Structure of unit cell FeO

1.2.2 Iron (lll) oxide, (Fe_2O_3):

Iron (lll) oxide is an inorganic compound having formula Fe_2O_3. It is one of the three fundamental types of iron oxide and has the important magnetic properties too. According to basic research point of view, iron (III) oxide is an appropriate compound for the general investigation of polymorphism, magnetic behaviour and structural phase transformation of nanoparticles. The presence of amorphous Fe_2O_3 and its four phases (alpha, beta, gamma and epsilon) is well-known [10].

1.2.2.1 Alpha phase:

Hematite (α-Fe_2O_3) consists of hexagonal (Rhombohedral) crystal system, constructed of iron atoms surrounded by 6 oxygen atoms. It is the main ore of iron, which exist as mineral hematite. At temperature below ~260 K, it behaves like antiferromagnetic and show weak ferromagnetic behaviour between 260 K and 950 K [11]. The rhombohedral system can also be considered as a cubic system extended along one body diagonal such that two interior points equally spaced along a diagonal, the Rhombohedral consists of three basis vectors of equal length and the angles α, β and γ are equal to each other, but are different from 90 degrees. Rhombohedral crystal picture below shows the stretch along one body diagonal.

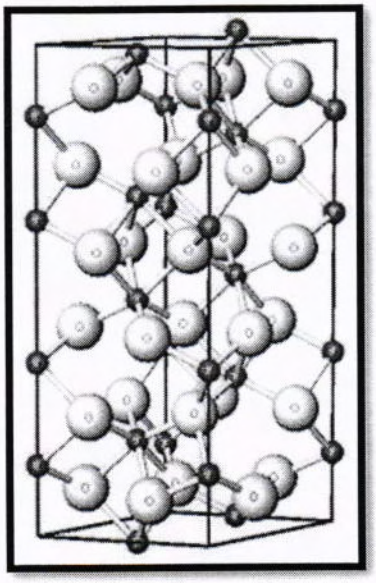

Figure 1.3: Structure of hematite, ferric ions F^{+3} in octahedral coordination (C.N. = 6) with oxygen ions O^{-2}

1.2.2.2 Beta Phase:

The β-phase of Fe_2O_3 has cubic bixbyite structure (body centred). There is a phase transition occurs from β-Fe_2O_3 to α-Fe_2O_3 about at temperatures above 500 °C. Different synthesis approaches i.e. pyrolysis of $FeCl_3$ solution, reduction of hematite by using carbon, or thermal decomposition of $Fe_2(SO_4)_3$, may lead to the formation of β-Fe_2O_3. It exhibits a paramagnetic behaviour.

1.2.2.3 Gamma phase:

Gamma Fe_2O_3 (maghemite) has a cubic structure and it has a dissimilarity from the inverse spinel structure of magnetite because of the presence of vacancies in Fe site with symmetry reduction. At room temperature, maghemite phase converts into hematite phase. [12]

Maghemite shows ferromagnetic behaviour and has many application in different fields i.e. recording tapes, [13] while ultrafine particles with less than 10 nm in size are superparamagnetic.

1.2.3 Iron (ll, lll) Oxide or Magnetite (Fe_3O_4):

Iron (II, III) oxide (magnetite) is the chemical compound having formula Fe_3O_4. It exists in nature as a mineral magnetite. It comprises of both Fe^{2+} and Fe^{3+} ions and sometimes it is expressed as $FeO \cdot Fe_2O_3$. It shows ferrimagnetic behaviour i.e. permanent magnetism, but sometimes incorrectly described as ferromagnetic. [14].

1.2.3.1 Ferrimagnetism in magnetite:

A ferrimagnetic material has permanent magnetism that occurs in solids in which number of atoms having magnetic moments that aligned in opposite directions, as in antiferromagnetism, though, these opposing magnetic moments are unequal, hence spontaneous magnetization remains [15]. It occurs when populations comprise of different materials (i.e. Fe^{2+} and Fe^{3+}). Ferrimagnetism mainly exists in magnetic oxides (ferrites). The magnetite (Fe_3O_4), is a ferrimagnetic material, before Néel's discovery of ferrimagnetism and antiferromagnetism, magnetite was considered as a ferromagnetic material. [16]

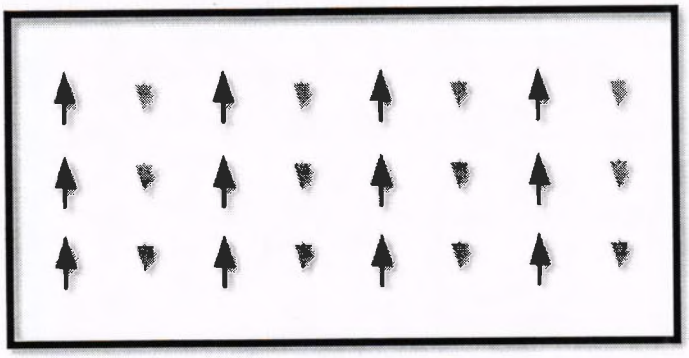

(a)

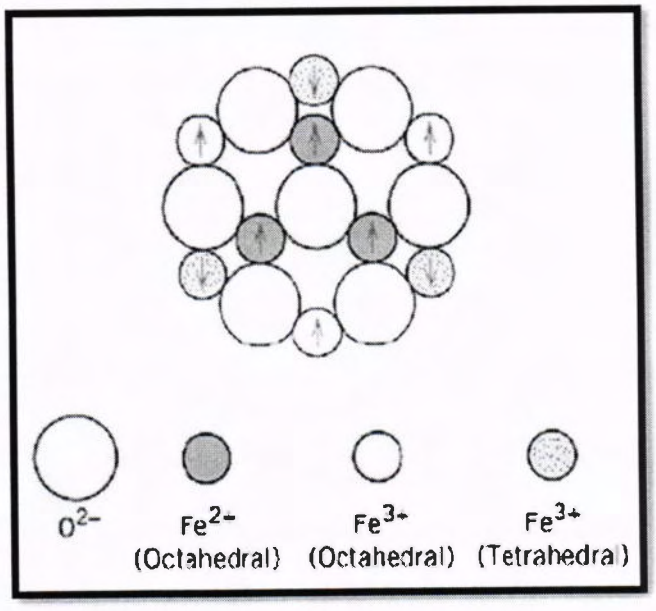

Figure 1.4: (a) Ferrimagnetism **(b)** Ferrimagnetism in magnetite

In above figure, all Fe^{+2} ions have spin magnetic moment in one direction. Half of Fe^{+3} ions have magnetic moment in one direction, the other have in another direction (decreasing the overall moment to just that contributed by the Fe^{+2} ions).

1.2.3.2 Structure of magnetite:

The electronic configuration of the Fe^{3+} ion is $1s^2\ 2s^2\ 2p^6\ 3s^2\ 3p^6\ 3d^5$ and Fe^{2+} ion is $1s^2\ 2s^2\ 2p^6\ 3s^2\ 3p^6\ 3d^6$ for Fe_3O_4 and γ-Fe_2O_3. The electronic, magnetic and spectroscopic properties are determined by the 3d electrons of Fe. Fe^{3+} has 5 unpaired electrons and Fe^{2+} has 2 paired and 4 unpaired electrons in the ground state.

Magnetite (Fe_3O_4) is a ferrimagnetic material and has an inverse spinel structure with 32 oxygen ions regularly cubic close packed in the [111] direction.

Fe^{+2} ions and half of the Fe^{+3} ions occupied by octahedral sites (where every Fe ion is bounded with six oxygen atoms) and the other half of the Fe^{+3} ions occupied by tetrahedral sites, it means one Fe^{+2} and Fe^{+3} ion occupied the octahedral sites, but tetrahedral sites are occupied by only Fe^{+3} ion as small ions tend to have low coordination.

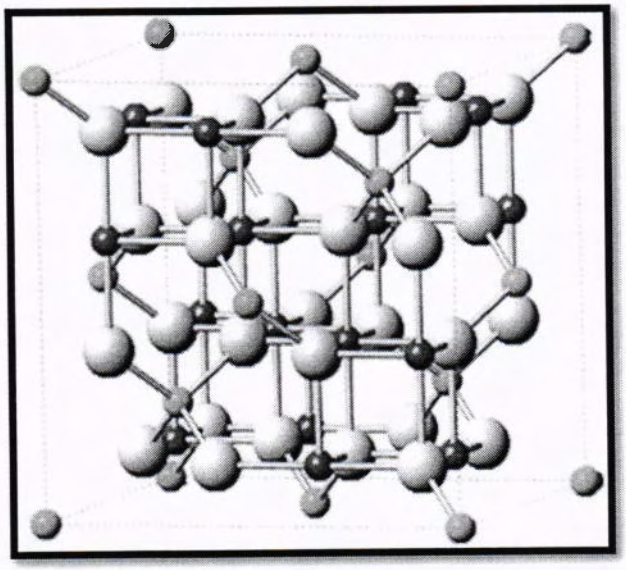

Figure 1.5: Crystal structure of magnetite (Fe_3O_4), green atoms represents Fe^{2+}, brown atoms are $Fe^{3+}$and white atoms are oxygen

1.3 Iron oxide nanoparticles:

Iron oxide nanoparticles have diameters between about 1 to 100 nm. Researchers has great interest in magnetic nanoparticles because of its amazing properties and biomedical applications [17].

1.3.1 Synthesis techniques of iron oxide nanoparticles:

Different synthesis techniques have been reported to obtain shape controlled, biocompatible, monodispersed and stable iron oxide nanoparticles. There are some common synthesis methods are listed below [18]:

- Co-precipitation method
- Thermal decomposition
- Hydrothermal method
- Sonochemical technique
- Electrochemical technique
- Laser pyrolysis technique

1.3.1.1 Co-precipitation method:

The co-precipitation method is the most common technique to synthesize maghemite (γ-Fe_2O_3) and magnetite (Fe_3O_4) nanoparticles. In this technique, ferric and ferrous ions dissolved in a highly basic medium with 1:2 molar ratios at the room temperature. Iron oxide NPs can be synthesized by using different precursors including iron chlorides, sulphates, perchlorates, nitrates etc. The size and shape of the particles depend on different factors e.g. PH value of the solution, temperature of the reaction, type of the precursor used, ratio of the precursors (ratio of ferric and ferrous ions), stirring rate, dropping rate of alkaline solution.

Kang et al have been reported the synthesis of narrow size distributional, uniform and monodispersed magnetite Fe_3O_4 NPs by co-precipitation without any surfactants having diameter 8.5 ± 1.3 nm. The molar ratio of Fe^{+2} / Fe^{+3} is 0.5 in an aqueous solution and PH is 11 to 12 [19].

Advantage:

- Simple and low cost method

Disadvantages:

- In reaction mixture, a high PH value is to be required during the synthesis and purification process.
- This method leads to the formation of particles with the large particle size distribution.

1.3.1.2 Thermal decomposition:

The thermal decomposition of $Fe(CO)_5$ by oxidation leads to the formation of high quality iron oxide NPs have been reported. This procedure requires a difficult operation and comparatively higher temperature. The nanostructures of α-Fe_2O_3 were successfully prepared by thermal decomposition of $Fe(NO_3)_3.9H_2O$.

Sun and Zeng have been synthesized the size controlled magnetite NPs by thermal decomposition of $Fe(acac)_3$ (acac = acetylacetonate) in phenyl ether at temperature 265 °C. A large size monodispersed iron oxide (Fe_3O_4) nanoparticles of 20 nm in diameter can be synthesized by using small iron oxide (Fe_3O_4) nanoparticles and these particles are dispersed in nonpolar solvent by seed mediated growth method. This procedure does not require a size-selection process. The prepared Fe_3O_4 nanoparticle can be transformed into γ-Fe_2O_3 nanoparticles by annealing at temperature 250 °C in the presence of oxygen for 2 hours [20,21]. The synthesis of iron NPs by the thermal decomposition of $Fe(CO)_5$ has been reported. The monodispersed γ-Fe_2O_3 NPs can also synthesize by following oxidation via chemical reagent [22].

Advantage:

- Size controlled monodispersed particles obtained with the narrow size distribution.

Disadvantage:

- The nanoparticles obtained via this method, are commonly dissolved only in the nonpolar solvents.
- It requires a comparatively very high temperature and complicated procedure.

1.3.1.3 Microemulsion:

The microemulsion is thermodynamically stable isotropic incapable mixture of two phase system (water and oil) under the certain condition i.e. surfactant, temperature and salt content. The surfactant particles form a single layer at interface between water and oil, with

hydrophobic head sites of surfactant particles dissolved in aqueous (water) phase and tails in oil phase. The Self-assembled assemblies of various types can be designed in different binary systems [23].

The microemulsion technique can be used in different application e.g. solvent free degreasing, in pharmaceutical industry, enhanced oil recovery etc.

Advantage:

- The resulting particles were small in size with higher saturation magnetization via microemulsion technique [24].

Disadvantage:

- Even with the use of surfactant, the aggregation of resulting nanoparticles need more washing procedures and several stabilization treatments.
- This method usually leads to the complicated procedure or may require high temperatures.

1.3.1.4 Hydrothermal method:

The controlled size and shape of magnetic nanoparticles are innovatively essential parameters because these parameters have a strong relationship with the magnetic properties. A hydrothermal technique comprises of numerous wet chemical technologies in which the crystallization of the material occurs in a closed container or vessel at high temperature (normally 130 to 250°C) and vapour pressure (normally 0.3 to 4 MPa).

Well crystalline grains and the dislocation free single crystal nanoparticles can be formed via hydrothermal technique [25].

Wang et al. [26] have been reported the single step method to make the highly crystalline nanoparticles without utilizing any surfactant via hydrothermal.

1.3.2 Green synthesis:

- In green synthesis, non-toxic entities like plants, leaves and roots, extract is used instead of chemicals.
- The phytochemicals in various plants contain carbohydrates, polyphenols, alkaloids, proteins, vitamins, sugars and phenolic acids, use as a metal reducing agent.

- Green synthesis is very useful in many fields, especially in agriculture, cosmetics, engineering and medical fields.

1.3.2.1 Metal nanoparticles synthesis using plant extract:

The three main phases occur during the synthesis of metal NPs by using the plant extract:

- The first phase is the activation phase, during which the metal ions reduced and then nucleation of reduced metal atoms happens.
- The next phase is growth phase, in which the small adjoining nanoparticles suddenly come together and form particles of a larger size.
- The third phase is termination phase, in which final shape of particles are determined [27].

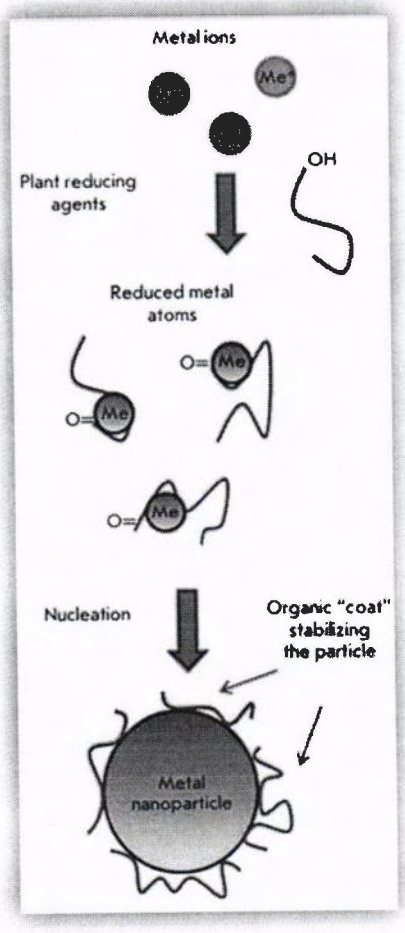

Figure 1.6: Mechanism of metal NP synthesis using plant extract

1.3.2.2 Advantages of green synthesis:

- The green synthesis of nanoparticles has been considered as a low cost, clean, rapid, environmental friendly and nontoxic method comparatively other methods.

- There is no need of the high energy, temperature, pressure or toxic chemicals.

1.3.3 Properties of iron oxide nanoparticles:

1.3.3.1 Thermal properties:

In a literature survey, magnetite's boiling and Melting point were detected at temperature about 2623 and 1590 °C, respectively. It showed Heats of decomposition, vaporization and fusion are 605, 298 and 138 KJ/mol, respectively [28].

1.3.3.2 Electrical properties:

As mentioned in previous studies, the ferric and ferrous ions occupied the octahedral sites, in the magnetite structure. The thermally delocalization of the electrons with these iron species are move inside the magnetite structure that starting high conductivity exchange constants with the ranging from -28 J·K to 3 J·K between tetrahedral/octahedral locations and octahedral/octahedral locations, respectively [29].

Verwey transition temperature (VTT) of magnetite (118 K) displays a well-ordered distribution of ferrous and ferric ions on the octahedral locations, impeding the delocalization of electron when the temperatures fall below VTT [30]. On octahedral locations, magnetite can be metal deficient to some extent because of electron delocalization effects. So, such type deficiency permits the magnetite for N and P type semiconductors. The resultant conductivities are in the range from 102–103 $\Omega^{-1}cm^{-1}$ [31].

The electrical conductivity of magnetite confirms the semiconductor behaviour and this conductivity value are very close to the metallic or conductor behaviour. As the energy bandgap values of insulators, conductors and semiconductors are >3, 0 and 0.2-0.3 eV respectively [32].

Magnetite has comparatively low energy bandgap i.e. 0.1 eV [33]. The energy bandgap of maghemite is 2 eV, which shows the insulator behaviour. The maghemite has curie temperature (Tc) about 900 K and magnetite has 860 K. At the Verwey transition temperature (T_V) about 120 K, magnetite displays the order-disorder transition, in which electrical conductivity diminishes. [34]

1.3.3.3 Optical properties:

Iron oxide has many interesting optical properties and important for designing electrochromic devices, photo electrochemical generation of hydrogen, solar radiation filters, etc. [35]. Magnetite and wustite shows the absorption in visible and near infrared region [36].

The maghemite and hematite do not show any absorption in near-IR region because they are insulators. The oxidation procedure of magnetite to the maghemite nanoparticles has been monitored by loss of the optical absorption in near infrared region [37]. The direct band gap of the hematite films is ranging from 2 to 2.27 eV, that is determined by the Tauc plots and indirect band gap is about 1.9 eV [38].

The direct band gap value of β-Fe_2O_3 films is 1.97 eV [39]. The bulk maghemite's band gap is 2 eV [40], whereas maghemite nanoparticles show an energy gap of 2.47 eV due to the quantum confinement effects. Magnetite's optical properties and band gap are related to quantum confinement phenomena. The physical and chemical properties varied with the size variation of nanoparticles. Through UV–Visible diffuse reflectance spectroscopy study it was observed magnetite nanoparticles of size range (20–25 nm) and (30-35) have band gap 2.12 ev and 2.05 ev respectively. The band gap variation is due to quantum size confinement [41].

The magnetite (Fe_3O_4) nanoparticles have photoluminescence spectra were recorded at room temperature which exhibited weak excitonic-emission in the UV region due to the recombination of free excitons, but in the visible range strong emission bands were observed that is caused by electronic transitions including defect-related energy levels in band gap of Fe_3O_4 nanoparticles. During synthesis of magnetite nanoparticles structural defects like oxygen vacancies can be produced because of the existence of few processes such as incomplete oxidation, rapid evaporation and fast crystallization. These defects may induce the creation of new energy levels in the band gap of Fe_{3O4} nanoparticles [42].

1.3.3.4 Magnetic properties:

It is reported that iron oxide nanoparticles often show superparamagnetic behaviour at room temperature when their size is less than 20 nm. Magnetite's Curie temperature (T_c) is 850 K, below this temperature (T_c) the magnetic moments are ferromagnetically aligned on the tetrahedral locations, as these locations are occupied by only ferric ions (Fe^{+3}). The magnetic moments are antiferromagnetically aligned on octahedral locations, as these locations are occupied by both ferrous(Fe^{+2}) and ferric(Fe^{+3}) ions. Such combined behaviour is called ferrimagnetic [43].

Therefore, the magnetite is ferrimagnetic at room temperature. Figure 1.8 (a) explains the ferromagnetic and antiferromagnetic behaviour on tetrahedral and octahedral sites respectively. As temperature increases, the aligned magnetic moments on tetrahedral locations will start to fluctuate and hence the ferrimagnetic strength will be reduced. When the

temperature achieved to curie temperature, then the magnetization becomes zero and superparamagnetic behaviour is detected. The coercivity of magnetite can be controlled during the precipitation process and the values of coercivity are ranging from 2.4-20 kAm^{-1}. The Coercivity is the magnitude of the applied magnetic field which is required for zero magnetization after the saturation magnetization point, as shown in figure 1.7 (hysteresis loop) [44].

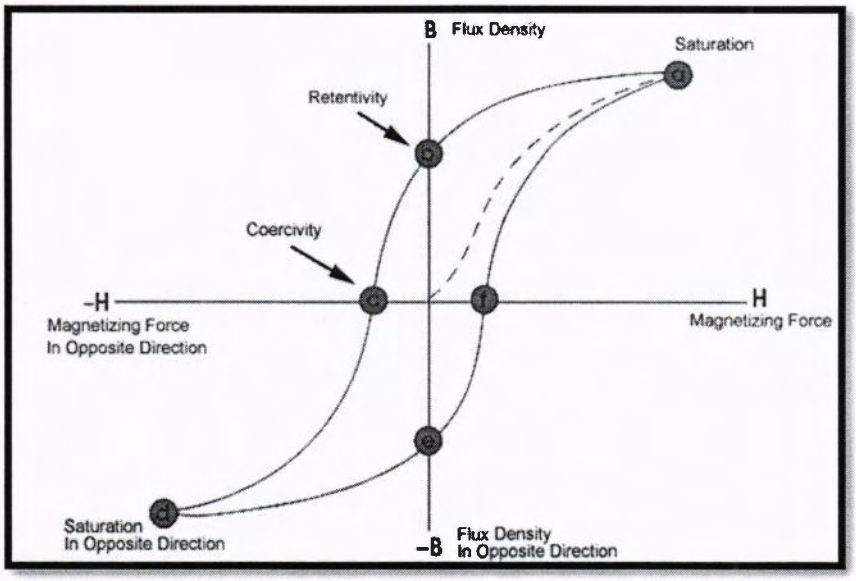

Figure 1.7: Hysteresis loop

The structure of hematite is rhombohedral and it shows the antiferromagnetic behaviour below its Morin transition temperature (T_M) about 260 K. It shows the weak ferromagnetic behaviour between T_M and T_N (Neel temperature about 948 K).

The weak ferromagnetic behaviour occurs due to a slight disorder of the antiparallel spin axis. In the basal plane the antiferromagnetic spins are indicated somewhat tilted, resulting in the small ferromagnetic moments. As the figure 1.8 (b) shows the rhombohedral and hexagonal unit cell with four ferric (Fe^{3+}) ions and oxygens connecting them.

It has been investigated that the particle size strongly depends on the Morin transition (T_M). The smaller particles have low Morin transition value. So, T_M depends on different factors including preparation method of the sample, O-H groups, addition of water and lattice defects in the hematite structure [45].

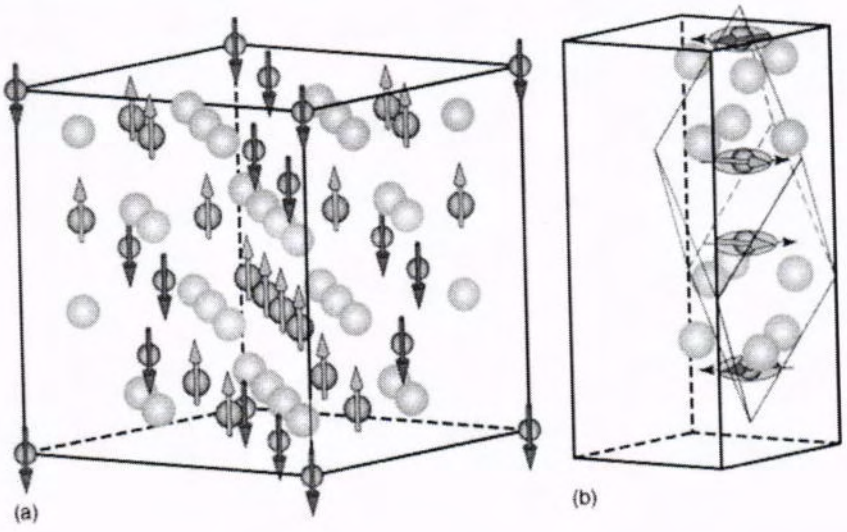

Figure 1.8: (a) Ferrimagnetic spin structure of magnetite, tetrahedral location occupied by Fe^{+3} ions with magnetic moments aligned along same direction (red down arrows), octahedral locations are occupied by Fe^{3+} and Fe^{2+} ions with unequal mixture of magnetic moments aligned in opposite direction (blue up arrows) **(b)** Weak ferromagnetism in hematite

The magnetic properties of hematite have linked to the size and shape of the nanoparticles. The coercivity (H_c) and the remanent magnetizations (M_r) and coercivity values of hematite are ranging from 0.6-16 memu/g and 31-530 O_e respectively [46].

The large sized particles of hematite have higher remanent magnetization and coercivity values and small particles of different morphologies have a single domain above blocking temperature (T_b), shows the superparamagnetic behaviour [47].

1.3.4 Applications of iron oxide nanoparticles:

In recent years, superparamagnetic iron oxides nanoparticles have been studied due to extensive applications in the field of nanoscience such as biotechnology, magnetocaloric refrigeration, in vivo biomedical field and ferrofluids [48].

The biomedical applications including tissue repair, magnetic resonance imaging (MRI) uses as a contrast agent, magnetically controlled drug delivery. It has been also investigated in other fields such as magnetic storage media and environment protection [49].

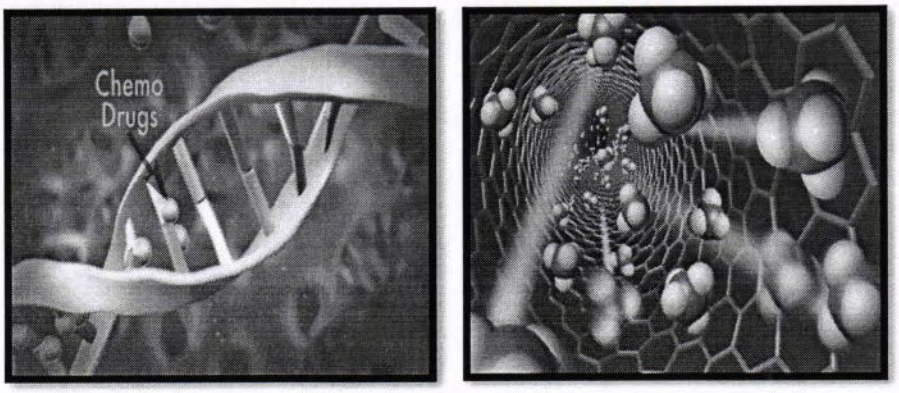

Figure 1.9: Drug loaded nanoparticles in drug delivery

1.3.4.1 Applications of magnetite, maghemite and hematite:

- Magnetite has great attention for researchers in biomedical applications because of their low toxicity and biocompatibility in human body.
- Superparamagentic magnetite nanoparticles used in the ferrofluids, initially it was planned for the high-performance seals in the space applications. The ferrofluid contains superparamagnetic nanoparticles that is spread in the organic media [50].
- Hematite and magnetite is used in industrial important applications including high temperature water gas shift reaction, desulfurization of natural gas, synthesis of ammonia (NH_3) and catalysis [51].
- The hematite nanoparticles are enormously beneficial in the photo catalysis, solar energy conversion, and water splitting treatment.
- Maghemite has also great consideration in biomedical field due to their low toxicity and biocompatibility, thus it is widely used biomedical applications like cancer therapy, magnetic resonance imaging, cell separation and magnetic induced hyperthermia etc [52].
- Maghemite is very useful in data storage and recording applications. To enhance its storage capacity and coercivity, the maghemite nanoparticles are coated with the cobalt (1-5%). The coated nanoparticles have higher thermal stability than the doped nanoparticles, with uniaxial magnetic anisotropy. So, these particles are used in magnetic discs, high bias audio tapes and video tapes etc [53]

Chapter No. 2

2 Literature review

Turmeric leaves were used to synthesize Iron oxide nanoparticles by calcination and microwave assisted method and characterized these nanoparticles by different techniques. As prepared nanoparticles were used to treat domestic wastewater in terms of orthophosphate (PO_4), Chemical oxygen Demand and Escherichia coli removal. Iron oxide nanoparticles by calcination Fe NPCal showed superior antimicrobial activity than Fe NPMw [54].

Metallic nanoparticles obtained via green synthesis method, in which eucalyptus extract was used for the reduction of metal ions. By using this extract well-formed magnetic nanoparticles are prepared and these nanoparticles are encapsulated in chitosan beads, which act as a magnetic hybrid material. The XRD pattern of these nanoparticles matched well with the structure of maghemite. The complete study of arsenic removal, these new magnetic hybrid materials are verified as good sorbent capacity [55].

Sada Venkateswarlu et al, synthsized the magnetite nanoparticles by using the extract of syzygium cumini seed. It is a nontoxic fruit and its extract is used as a reducing agent. Sodium acetate is used as stabilizing agent. Then prepared anaoparticles were characterized via different techniques including X-ray diffraction (XRD), transmission electron microscopy (TEM), Raman spectroscopy, Vibrating sample magnetometer (VSM), Energy-dispersive spectroscopy (EDS), FTIR spectroscopy. The XRD results showed the particles are magnetite with inverse spinel structure. TEM images showed the spherical morphology of particles. VSM results indicated the ferromagnetic behaviour of the magnetite nanoparticles with saturation magnetization 13.6 emu/g [56].

Magnetite (Fe_3O_4) NPs were synthesized by a novel method, in which non-toxic extract of watermelon rind is used as a capping and reducing agent. As prepared Fe_3O_4 nanoparticles were characterized via different techniques containing, Fourier transform infrared spectroscopy (FTIR), transmission electron microscopy (TEM), vibrating sample magnetometer (VSM), X-ray diffraction (XRD). The X-RD investigation showed the highly crystalline and face centered cubic structure of iron oxide. The FTIR results revealed that these particles are stabilized by capping agent. It is a simple, pollutant free and cheap method to synthesize the magnetic

nanoparticles. As prepared nanoparticles are small in size with the narrow size distribution from 2-20 nm and shows wonderful magnetic behaviour with saturation magnetization of about 14.2 emu/g. Then these nanoparticles were used as a catalyst [57].

The Iron oxide nanoparticles (IONs) were synthesized by the co-precipitation method in air atmosphere from the ferrous aqueous. The effect on properties of the nanoparticles by changing ratio of [Fe^{+2}/Fe^{+3}] were investigated. Fourier transform infrared spectroscopy and X-Ray diffraction confirmed the formation of iron oxide. VSM analysis shows that the saturation magnetization increased from 37.6-59.4 emu/g by increasing the ratio of [Fe^{+2}]/[Fe^{+3}] from 1/2-6/6, and particles are superparamagnetic having zero coercivity. Then the particles start to show coercivities (8Oe,22Oe and 33Oe) with the increase of the ratio above 6/6 and increases upto74.3 emu/g. Hence, it is concluded that the magnetic properties and the particle size of nanoparticles mainly depends on the [Fe^{+2}]/[Fe^{+3}] ratios. It is observed that particles are less than 11 nm in size with zero coercivity and showed superparamagnetic behaviour [58].

An advanced quantitative synthetic method for preparing magnetite nanoparticles was attained via co-precipitation method, in which only one iron precursor is used. For the first time, the molar ratios (2:1) of Fe(III): Fe(II) was achieved in the solution by using potassium iodide (KI) for the reduction of Fe(III). By following the filtering process the iodine is formed and then this filtrate was hydrolyzed with 25% of NH_4OH (ammonium hydroxide) solution at PH 9 to 11. As the synthesized magnetic nanoparticles were characterized via different techniques, including field emission scanning electron microscopy (FESEM), Fourier transform infrared spectroscopy, X-ray diffraction, field emission transmission electron microscopy (FETEM) and selected area electron diffraction (SAED). The average diameter of magnetite nanocrystals was 7.84 ± 0.05 nm and for magnetite nanorods 6.3 ± 0.2 nm [59].

B. Kumar, L.Cumbal. et al. have synthesized iron oxide nanoparticles by a low-cost method, in which extract of passiflora tripartia var. mollissima is used. Then prepared nanoparticles were characterized via different techniques containing VSM, UV visible, Transmission electron microscopy and Dynanamic light scattering. The analysis revealed that the particles are 22.3± 3 nm in size with spherical shape. The synthesized nanoparticles were used as a catalyst. The reaction was carried out under mild condition with good yields. without significant loss of activity, the catalyst is easily separated by magnet and recyclable [60].

It was reported that synthesis of magnetic iron nanoparticles has great consideration due to its tremendous properties especially magnetic properties became the attention for researchers. These properties are valuable in different biomedical applications like drug loading, medical diagnoses and beneficial in the technological areas. Depending on the crystal structure Fe_2O_3 has different phases, namely, α, β, γ and ε phase. The Hematite (α-Fe_2O_3) has hexagonal (Rhombohedral) crystal system. The gamma phase Fe_2O_3 is known as maghemite. It remains in this phase at low temperature. It has cubic structure when the size of particles is less than 8 nm and it will be transformed into alpha phase at higher temperature. The β-Fe_2O_3 phase exists in metastable with primitive hexagonal structure and it converts into α-Fe_2O_3 at high temperature about 500° C. The ε-Fe_2O_3 has intermediate state between γ and α with orthorhombic structure. This phase converts into to α phase at temperature between 500 to 750 °C. The ferromagnetic behaviour is observed in γ-Fe_2O_3 and ε-Fe_2O_3. The antiferromagnetic and paramagnetic behaviour observed in α-Fe_2O_3 and β-Fe_2O_3 respectively [61].

Synthesis of nanoparticles by chemical procedures involve toxic solvents, which could produce unsafe and hazardous by-products causing high energy consumption also. Due to low toxicity of magnetic iron oxide nanoparticles have become the primary materials for the biomedical applications. Iron oxides NPs like magnetite (Fe_3O_4) and maghemite (γ-Fe_2O_3) used as potential components in biomaterials due to their low toxicity [62].

There are number of medical applications have been found for iron oxide nanoparticles, including drug targeting, bio separation processes and cancer chemotherapy. The biologically differing marine environment is the great promise for nanotechnology and the nanoscience. In palliative treatment of prostatic carcinoma, an effective non-steroidal anti androgen, Flutamide has been used [63].

Treatment with flutamide may cause different side-effects such as diarrhea, tiredness, weakness, breast fullness and liver malfunction. The important and cost-effective development procedures for preparation of sustained release formulations in the industrial scale. For this purpose, we successfully formulated with biosynthesized iron oxide nanoparticles. However, using seaweeds for the synthesis of nanoparticles, only few reports are available till date. Sangeetha N*, A. K. Kumaraguru synthesized iron oxide nanoparticles from freshly collected seaweeds. The synthesis was optimized under various physico-chemical parameters such as, reaction temperature, reaction pH, and time. Further, these synthesized nanoparticles (NPs) was characterized by various techniques i.e. Atomic Absorption spectrometry measurements,

transmission electron microscopy (TEM), Scanning electron Microscopy (SEM), Fourier transform infrared spectroscopy (FTIR) and Energy Dispersive X-Ray (EDX) analysis. The biosynthesized iron oxide nanoparticles were also studied in drug delivery [64].

From two different families, stems and leaves of three different herbs has been used to examined the the bioactivity and phenolic contents of the extracts. were used to phenolic compounds and the bioactivity of the extract by using their antioxidant activity or DPPH scavenging ability. Mint leaves belongs to the Lamiaceae family. The antioxidant activity and the total phenolic compounds in mint leaves extract are 34.21% and 1.24 mgGAE/100 mL respectively. These values show that mint leaves extract have higher antioxidant activities and phenolic compound than parsley and coriander extract. As the coriander and parsley belongs to the family of Apiaceae. It was also investigated that leaves have higher quantity of phenols and more antioxidant activities than the other parts like stems [65].

Runnie et al investigated the existence of phenolic contents and antioxidant activities in the mint leaves and examined these effects in the rats. The extract of parsley also showed the antioxidant activities. The coriander and parsley exists in the Apiaceae family and mint has Lamiaceae family. The values of antioxidant activities and phenolic contents may differ in different parts of these herbs, as the stem parts of the same plant have lower phenolic contents than the leaves. The properties of the plants may also differ in different environmental condition or geographical areas [66].

Dragana M et al examined the content of total phenols and flavonoids and the antioxidant activities of different dried herbs. These herbs were dried in different ways and then observed the antioxidant activities of the extract. The mint leaves were dried at 45°C in the oven and in open atmosphere. Then compared the phenolic contents, antioxidant activities and flavonoids in the extracts of these dried herbs. It showed that naturally dried herb has high yield of the extract and herbs dried in low temperature condensation drying oven had low yield extract. The total phenolic contents were determined by spectrophotometric methods and flavonoids was determined by complexation reaction. The naturally dried herbs contain the highest phenolic contents, flavonoids and antioxidant activities than the extract of herbs dried in laboratory oven [67].

It has been reported, magnetic iron nanoparticles are synthesized via co-precipitation method by using the aqueous solution of ferrous in the air atmosphere. The effect of the molar ratios of $[Fe^{+2}]/[Fe^{+3}]$ on different properties of the magnetic iron nanoparticles has been

investigated. The prepared particles were characterized via different techniques. The iron oxide's characteristic peaks were observed via X-Ray diffraction and fourier transform infrared spectroscopy analysis showed the presence of iron oxide particles. Magnetic behaviour of magnetic nanoparticles was observed by vibrating sample magnetometer which shows that the saturation magnetization is increased from 37.5-59 emu/g as the molar ratios of $[Fe^{+2}]/[Fe^{+3}]$ increased from 1/2- 6/6. These particles showed the superparamagnetic behaviour with zero coercivities. However, the samples started to show the coercivities by increasing the ratios above 6/6 (8Oe,22Oe and 33Oe). The Particle size are calculated by X-Ray diffraction, vibrating sample magnetometer and transmission electron microscopy. The all values obtained via different techniques are almost same. It was also observed that the molar ratios of $[Fe^{+2}]/[Fe^{+3}]$ has significant effects on the magnetic properties of the nanoparticles. The particles showed the superparamagnetic behaviour with zero coercivity when size of these particles are less than 11 nm [68].

For the synthesis of desired magnetic nanoparticles, a low-cost co-precipitation method is followed. Basically, in co-precipitation method, nanoparticles of iron oxide are prepared by using the iron precursors and alkaline solution as a reducing agent. Iron salt solution maintained at continuous stirring with the addition of alkaline solution. The properties of nanoparticles can be altered by changing the number of factors including the pH values, temperature of reaction and the ratios of the metal ions [69].

CHAPTER No.3

3 Experimental work

3.1 Synthesis of iron oxide nanoparticles:

Iron oxide nanoparticles are synthesized by Co-precipitation method.

3.2 Apparatus used:

- Magnetic stirrer
- Mechanical stirrer
- Heating plate
- Beaker
- Ultrasonic bath
- Furnace
- Funnel
- Whatman filter paper
- Spatula
- Centrifuge machine
- Centrifuge tube
- Permanent magnet
- Weight balance

3.3 Material used for chemical method:

- Iron chloride ($FeCl_3$)
- Iron sulphate ($FeSO_4$)
- Hydrochloric acid (HCl)
- Ammonium hydroxide (NH_4OH)

3.4 Procedure:

- For the synthesis of magnetite (Fe_3O_4) nanoparticles, firstly 3.05g ferric chloride ($FeCl_3$) and 2.1g ferrous sulphate ($FeSO_4$) dissolved in 25 ml distilled water with continuous stirring for one hour.
- Then few drops of HCl were added to the above mixture at 85 °C and stirred strongly at 1500 rpm for one hour.

- Then 7ml of ammonium hydroxide (NH_4OH) was added drop wise into the solution and stirring kept slow for around one hour. Thus, the colour of solution was changed from light orange to black, which indicate that the formation of magnetite (Fe_3O_4) nanoparticles.

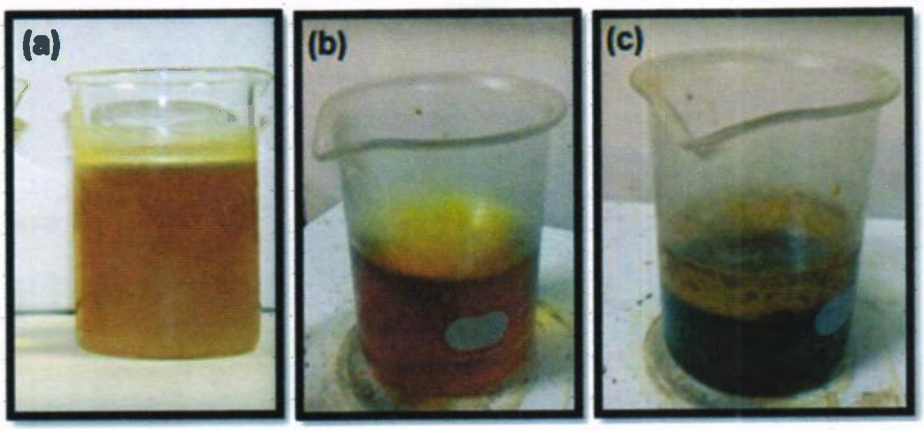

Figure 3.1: (a) solution of $FeCl_3$ and $FeSO_4$ in 25 ml distilled water, **(b)** after adding a few drop of HCl, **(c)** After adding 7 ml of NH_4OH

- The as-synthesized Fe_3O_4-NPs were separated by applying external magnetic field.

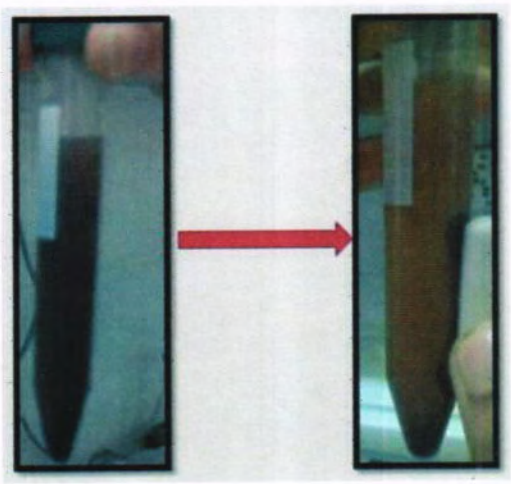

Figure 3.2: Before and after applying external magnetic field

- These particles were washed for several times with the distilled water and ethanol and then dried.

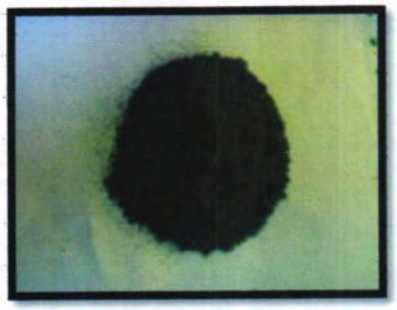

Figure 3.3: Dried magnetite nanoparticles

Chemical reaction:

The chemical equation of Fe_3O_4 nanoparticles formation may be written as:

$$2Fe^{+3} + Fe^{+2} + 8OH^- \rightarrow Fe_3O_4 + 4H_2O$$

3.5 Green synthesis:

Iron oxide nanoparticles are synthesized by using extract of three different plants.

3.5.1 Materials and Method:

The metal precursors used in this experiment were iron chloride ($FeCl_3$) and iron sulphate ($FeSO_4$). Three plants (mint, spinach, ginger) purchased from market. The extract of these plants is used as a stabilizing, capping and reducing agent for the synthesis of iron oxide NPs.

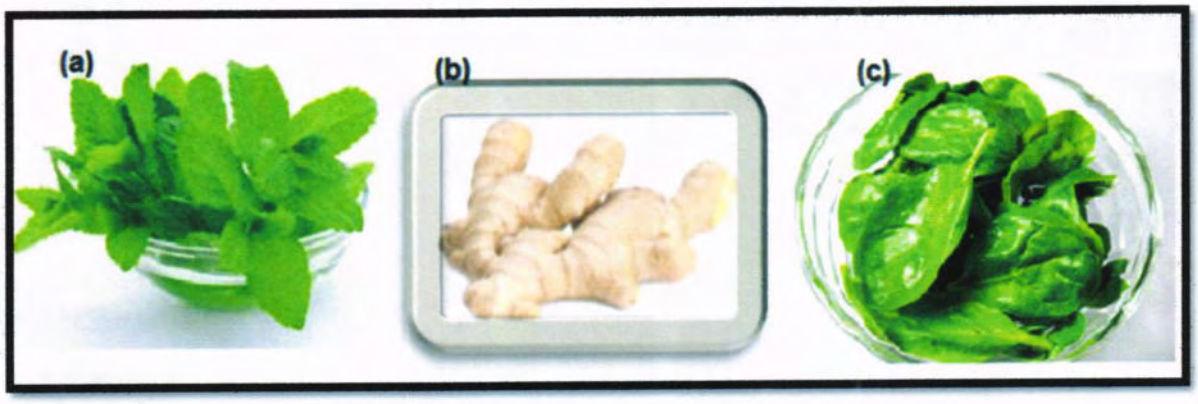

Figure 3.4: (a) mint leaves (P_1), **(b)** ginger (P_2), **(c)** spinach leaves (P_3)

3.5.2 Preparation of extract:

10 grams of ginger, mint leaves and spinach leaves were thoroughly washed with the help of de-ionized water and then dry at the room temperature for few hours. Extract prepared

by adding chopped mint leaves in 200 ml distilled water and mixture was heated at 80 °C for 2 hours. The same process was repeated with ginger and spinach for extract preparation. Thus, colour of mixture was changed from watery to pale yellow or light green.

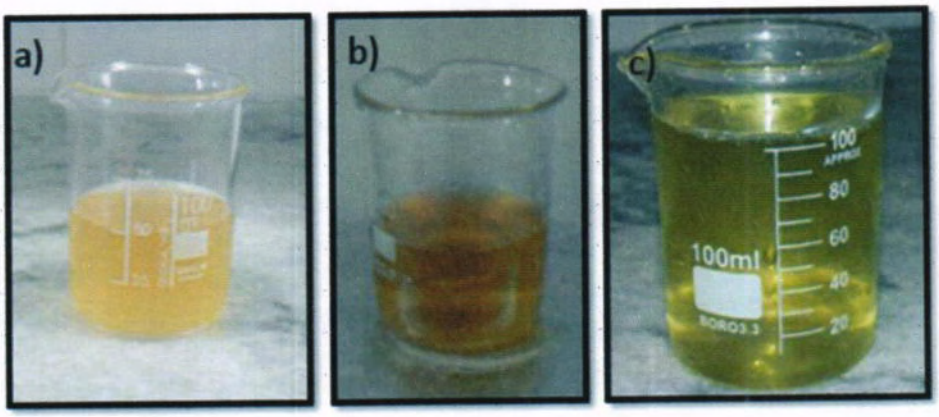

Figure 3.5: (a) Ginger extract, **(b)** mint leaves extract, **(c)** spinach leaves extract

Then extract was filtered through a whatman filter paper and stored at -4° C for further use.

3.5.3 Synthesis of iron oxide nanoparticles:

Iron oxide nanoparticles are synthesized by using plant extract in two ways.

3.5.3.1 Method 1:

- Firstly 2.1g $FeSO_4$ and 3.05g $FeCl_3$ was dissolved in 25 ml of distilled water with the help of continuous stirring for one hour at room temperature.
- After one hour, 7 ml of alkaline solution (extract) was added drop wise into the above mixture.
- During the addition of alkaline solution, mixture was maintained at 80 °C with constant stirring for the formation of precipitates.
- On the addition of alkaline solution, immediately changed in colour of solution was observed from pale yellow to black, which indicates the formation of magnetite NPs.
- Then cool down the solution for few hours at room temperature.
- The same procedure was followed with ginger and spinach leaves extract.

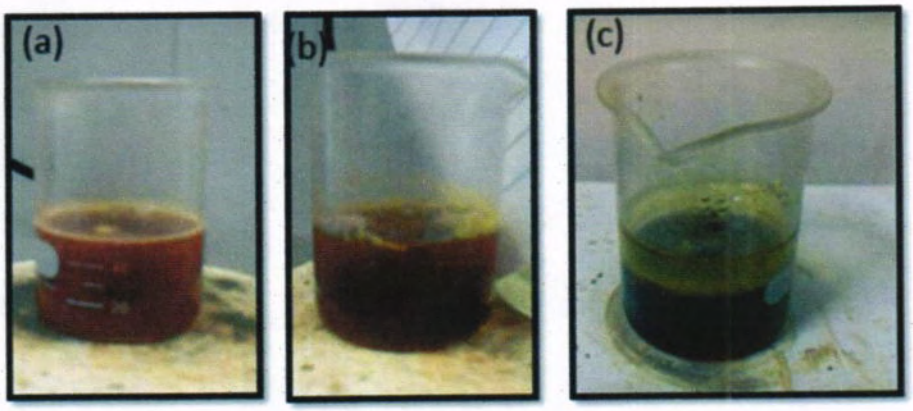

Figure 3.6: (a) solution of $FeCl_3$ and $FeSO_4$ in 25 ml distilled water, **(b)** After adding few drops of extract, colour of solution turned into dark brown, **(c)** after adding 7 ml of extract, colour of solution turned into black

- After that, iron oxide nanoparticles were separated by using a permanent magnet.

Figure 3.7: After applying external magnetic field

- These particles were washed with distilled water and ethanol and then dried.

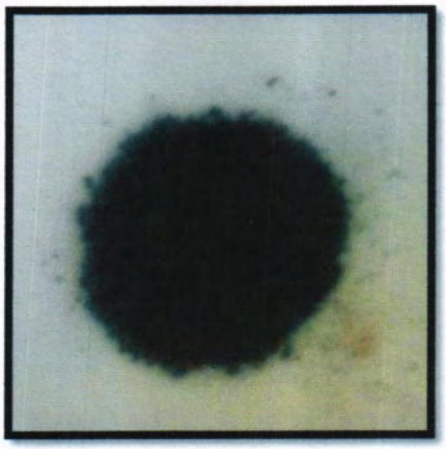

Figure 3.8: Black powder of iron oxide nanoparticles

3.5.3.2 Method 2:

- 2.1g $FeSO_4$ and 3.05g $FeCl_3$ was dissolved in 25 ml of mint extract with the help of continuous stirring for 3 hours at 80 °C.
- The colour of solution was immediately changed from yellow to black, which indicates the formation of magnetite (Fe_3O_4) NPs.
- The cool down the above solution for few hours at the room temperature and separate the magnetite nanoparticles with external magnetic field.
- Then washed and dried these nanoparticles.

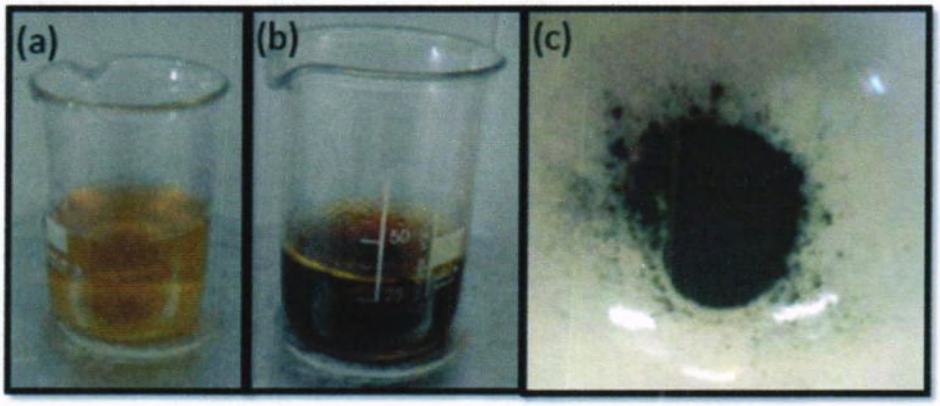

Figure 3.9: (a) 25 ml of mint extract, **(b)** $FeSO_4$ and $FeCl_3$ in extract, **(c)** Black powder of iron oxide nanoparticles

3.6 Characterization tools:

- For studying the crystallographic properties, X-ray diffraction (XRD) measurements have done with the Rigaku apparatus (Cu Kα1 radiation, $\lambda = 1.54056$ Å) operated at room temperature with 40KV and 100mA. For wide angle XRD, 15°-60° angular range was used for recording of diffraction patterns.
- Fourier transform infrared spectrometer was used for recording of FTIR spectra of the samples.
- Scanning electron microscope (SEM) results were obtained from JEOL 6400 instrument.

Chapter No.4

4 Results and discussion

4.1 Metal reduction mechanism:

Spinach, mint and ginger are the well-known functional foods because of their richness in minerals, lipids, certain vitamins, and several bioactive constituents such as polysaccharides, proteins and polyphones. So, their phytochemicals comprise of carboxyl, hydroxyl and amino functional groups, which can act as effective metal-reducing agents.

Extracts of spinach and mint leaves have higher quantity of phenolic contents and more antioxidant activities than the extract of other parts like stems [70].

The antioxidant components analysed in ginger, were polyphenols, vitamin C, β carotene, flavonoids and tannins [71]. Phytochemical components in yellow ginger is higher than white ginger [72].

The polysaccharides, as a major component consists in above three plants, which has glucose, hydroxyl, fructose and aldehyde group may cause reduction of the metal precursors.

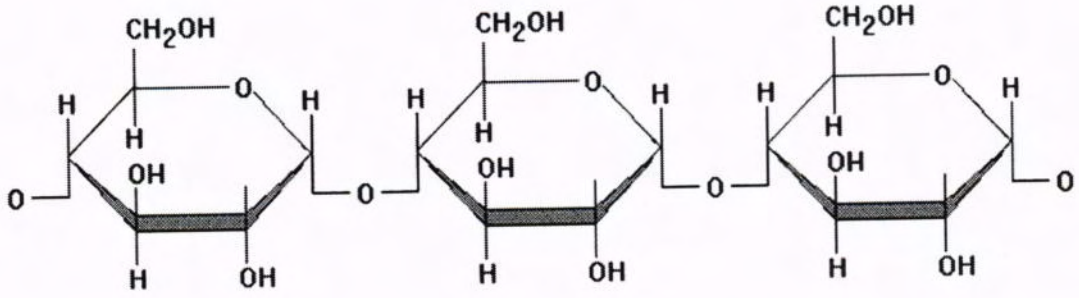

Figure 4.1: structure of polysaccharides

The reduction process may complete in two steps:

- In the first step, the metal precursor is added in the extract and forms a complex. Then it makes a partial bond with the metal ion by breaking of -OH bond.
- In second step, partial bonds will break and then metal ions reduces by transferring of electrons thus nanoparticles will have formed.

The iron nanoparticles are very unstable that is why it will get reduced to iron oxide nanoparticles in the short duration of time. During this process, the aldehyde groups (organic compounds) are oxidized very quickly to the corresponding acids [73].

4.2 X-Ray Diffraction Spectroscopy:

The crystalline structure, crystalline size and presence or absence of impurity phases of iron oxide nanoparticles are investigated by XRD.

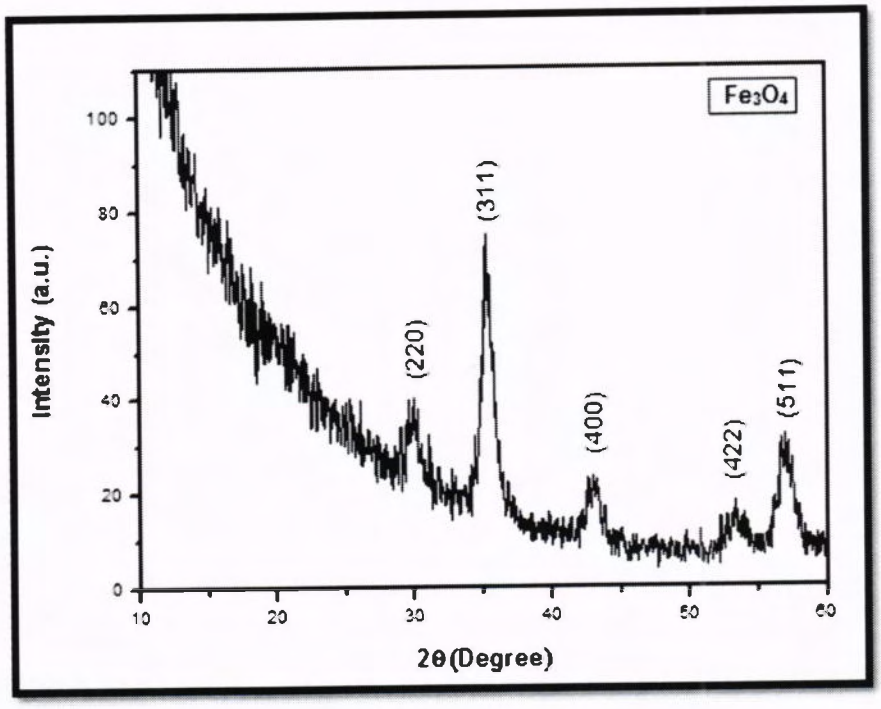

Figure 4.2: XRD pattern of Fe_3O_4 NPs by chemical synthesis

As X-ray diffraction pattern lies in the limit of 15 to 60 degrees. In figure 4.2, five representative peaks at $2\theta = 30°$, 35.4°, 43.1°, 53.2°corresponds to the plane (220), (311), (400), (422) respectively. There is no peak occurred due to impurity and other phases of iron oxide. This specifies the formation of magnetite (Fe_3O_4) nanoparticles with inverse spinel structure. The peak positions and relative intensities of all diffraction peaks matched well with the JCPDS card No. 86-1359 which is the authenticated data for magnetite (Fe_3O_4). The peaks are more intensive and narrow which indicates the good crystalline structure of magnetite nanoparticles [74]

The crystallite size of prepared nanoparticles is obtained from the broadening of peak indexed at (311) using Debye - scherrer formula:

$$d = k \lambda / \beta \cos\theta$$

Where "d" is the crystallite size, "β" is the full width at half maximum, "k" is the scherrer constant (0.9), "λ" is wavelength of X-rays (0.154 nm) and "θ" is Bragg's angle [75].

Crystallite size calculated for the iron oxide nanoparticles synthesized by chemical method is 17 nm.

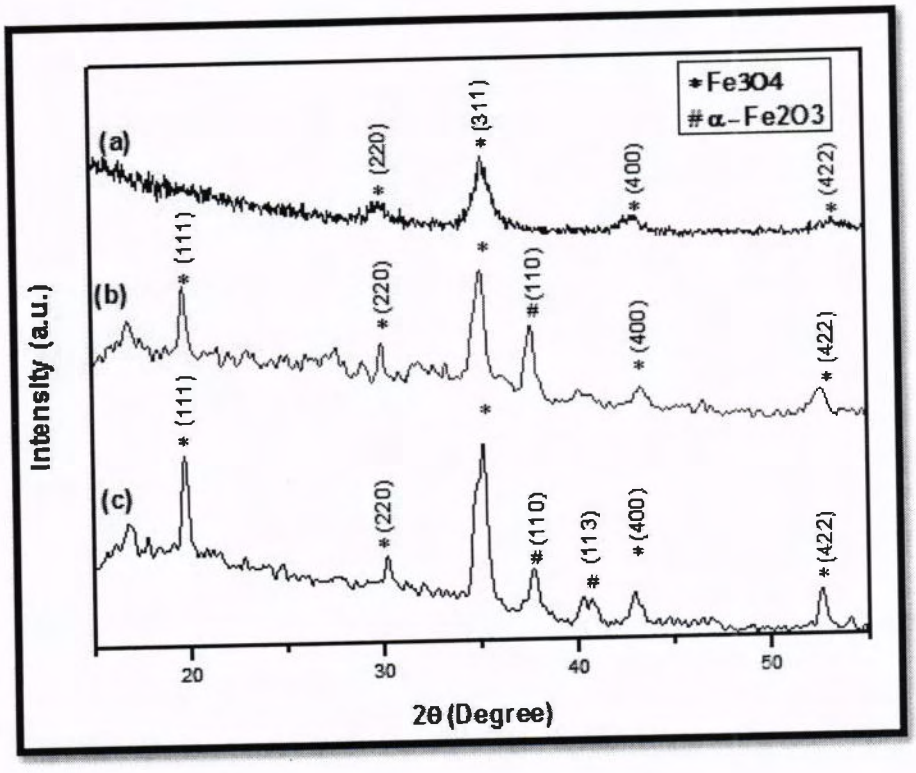

Figure 4.3: Comparative XRD Pattern of iron oxide NP's **(a)** chemical synthesis **(b)** Green synthesis using 7 ml of mint extract (M_1) **(c)** 25 ml of mint extract (M_2)

Chemically synthesized magnetite nanoparticles have good crystalline structure without calcination at higher temperature as shown in figure 4.2 (a), and samples prepared by green synthesis gave an amorphous spectrum without calcination. So, these samples are needed to calcine at higher temperature in furnace.

Figure 4.3 (b) and (c) shows that the XRD pattern of iron oxide nanoparticles synthesized by method 1 and method 2 respectively. Five characteristic peaks of Fe_3O_4 are observed at 2θ = 19.6°, 30°, 35°, 43.3°, 52.9° corresponds to the plane (111), (220), (311), (400), (422) respectively and two peaks of α-Fe_2O_3 are observed at 2θ = 37.6° and 40.3°.

The peaks of α-Fe_2O_3 arises in M_1 and M_2 due to calcination at 300 °C. At this temperature magnetite begin to convert in hematite [76]. The crystallite size of M_1 and M_2 is

18 and 19.5 nm respectively. As careful inspection of the above results, there is no change occurred in crystal structure, only crystallite size increased by changing method as shown in the figure 4.3 (b) and (c).

But the other two samples prepared by ginger and spinach leaves extract, still have an amorphous spectrum after calcination at 300 °C.

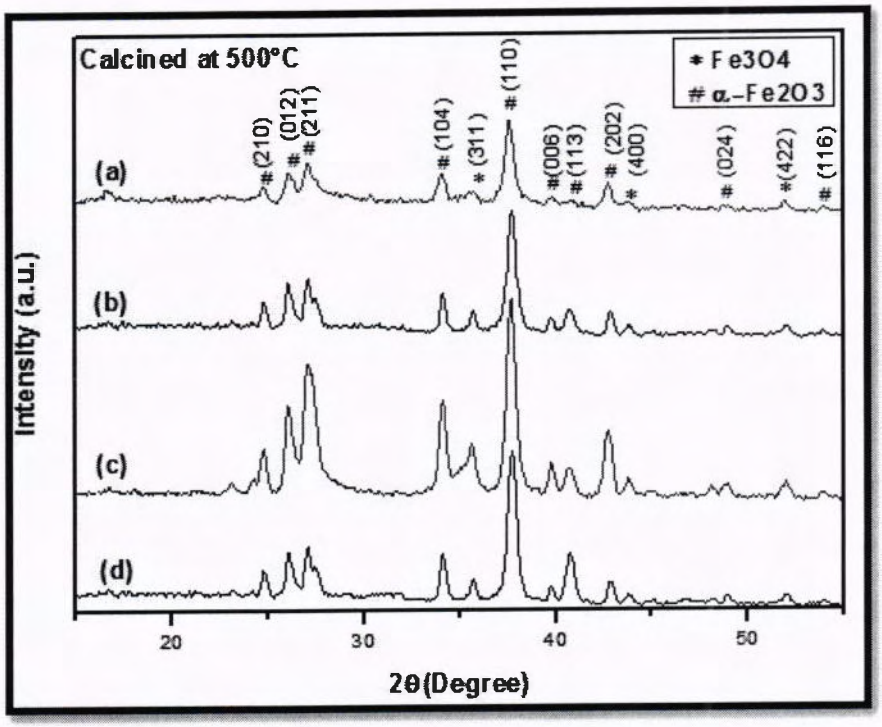

Figure 4.4: XRD pattern of iron oxide NP's calcined at 500 °C (a) chemical synthesis (b) using mint leaves extract P_1 (c) Ginger extract P_2 (d) Spinach leaves extract P_3

It is observed that on increasing the calcination temperature, the nanoparticles endure the complete decomposition, and then hematite phase develops along with the magnetite (Fe_3O_4) phase. At temperature 300 °C, only few peaks of hematite showed and at higher temperature the phase transformation more proceeded to the hematite phase. Above 300 °C, α phase iron oxide nanoparticles dominate diffractogram. Hence, the above discussion revealed that at higher calcination temperature about 500 °C Fe_3O_4 transformed into α-Fe_2O_3 [77]. The formation of the hematite (α-Fe_2O_3) phase is favoured at the higher temperatures [78].

It also observed that the samples were calcined at low temperature have broadened peaks and signifying the small crystallite size [79]. As the temperature increased, the reflections

coming from the sample became sharper and signifying the large crystallite size with the decrease of full width half maximum [80].

The increase in size of crystallite may affect the stoichiometry ratios and the structure of nanoparticles or may cause total phase transformation [81]. The phase conversion with the increase of crystallite size generally occurs to acquire a stable phase of particles via nanomizing the surface energy. As hematite is the most stable phase comparatively to the other phases of iron oxide which has higher enthalpy of formation under the aerobic conditions [82].

4.3 Morphological Investigation of NPs via SEM:

Surface morphology of iron oxide nanoparticles were analysed by scanning electron microscopy.

4.3.1 SEM analysis of iron oxide NPs via chemical synthesis:

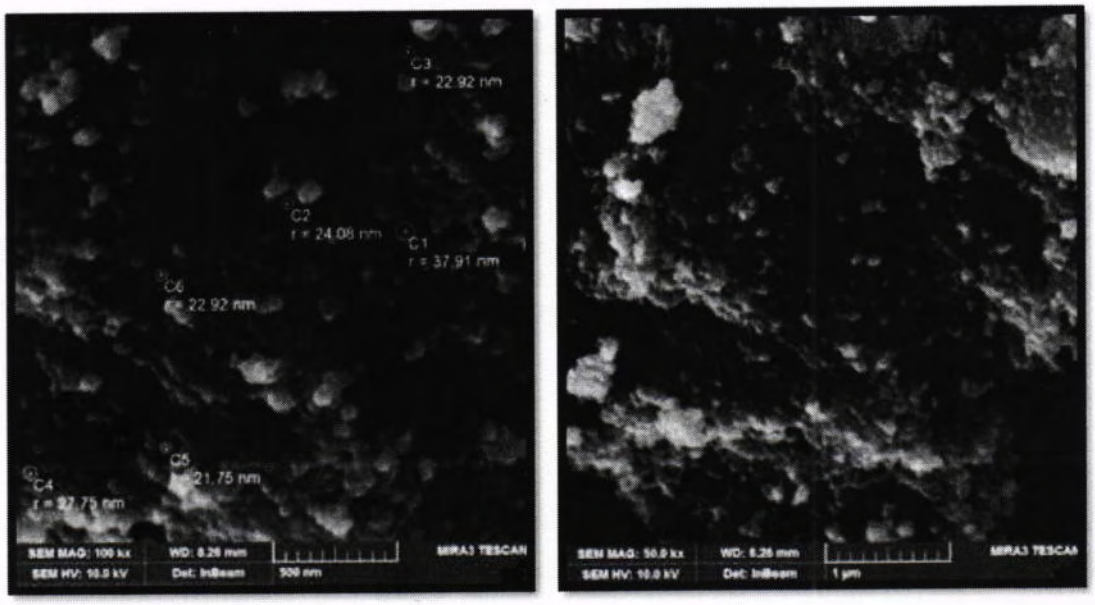

Figure 4.5: SEM images of chemically synthesized iron oxide nanoparticles

Scanning electron microscopy gives the images of samples with high resolution at nanoscale and determine the morphology of nanomaterials. Figure 4.5 shows the images of iron oxide nanoparticles at magnifications of 50,000 and 100,000. The average particle size is about 22 nm with spherical morphology. The particles are agglomerated due to magnetic dipole-dipole interactions among the nanoparticles. The nanoparticles are well defined with non-homogenous distribution.

Preparation of spherical magnetite nanoparticles has also been reported previously by Mamani, J.B., A.J. Costa-Filho, et al., with multiple dispersion. They synthesized iron oxide nanoparticles with average diameter of about 9 nm [83].

Feng, L., M. Cao, et al., demonstrated the high surface area magnetite nanoparticles with superparamagnetic property, because they obtained the particles with very small size distribution of nearly 10 nm and observed an agglomeration in Fe_3O_4 nanoparticles [84].

4.3.2 SEM analysis of iron oxide NPs via Green synthesis:

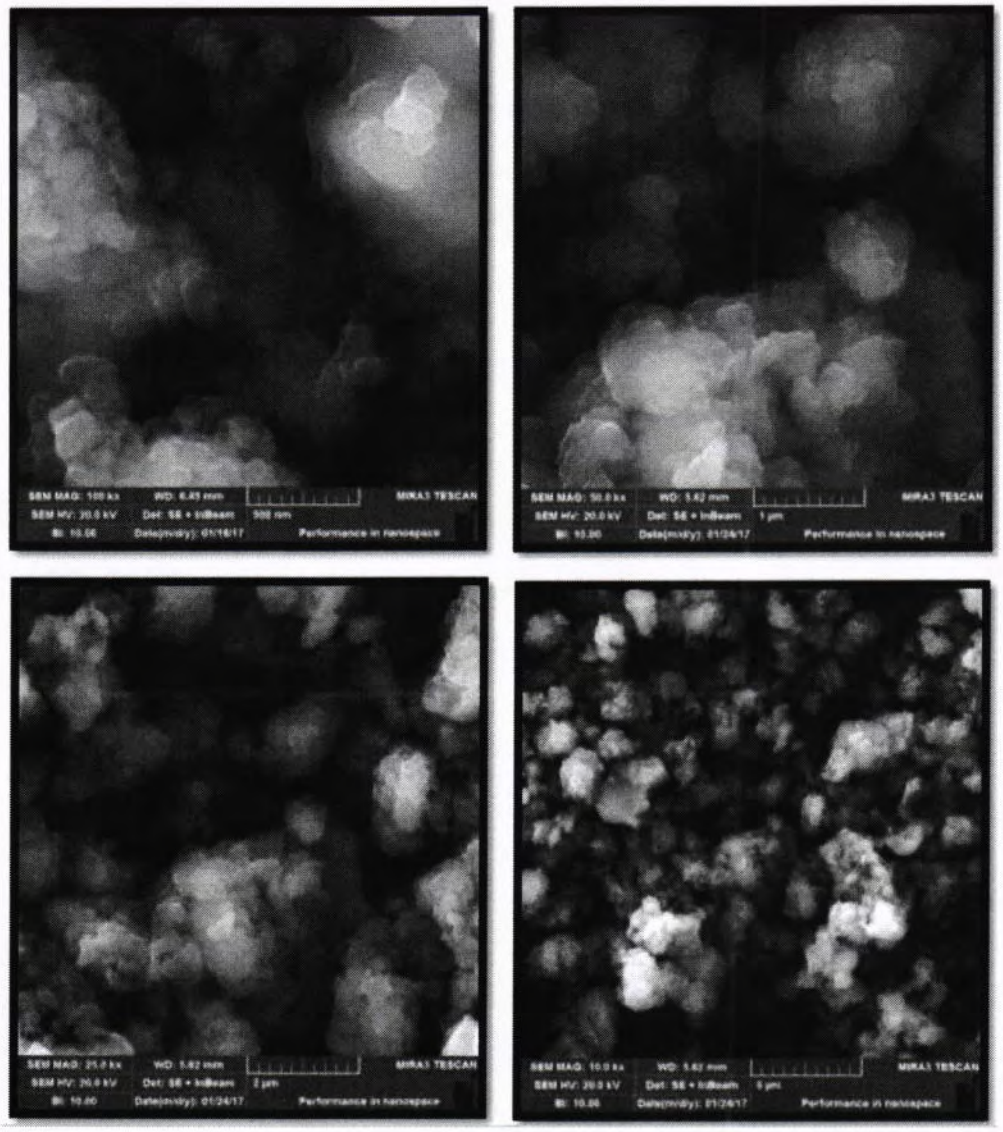

Figure 4.6: SEM images of iron oxide NPs (prepared by using 7 ml of mint extract) at different magnification

These images show that the particles are agglomerated because of thickening properties in the plan extract or might be the presence of O-H group (hydroxyl group) from extracts. The agglomeration could be prevented by using oleic acid [85].

The tendency of agglomeration is not astonishing as synthesized Iron oxide NPs are small in size and also possess the magnetic properties [86]. The dispersion of these nanoparticles are observed in plant matrix [54].

The particles are less than 100 nm in size with roughly spherical morphology.

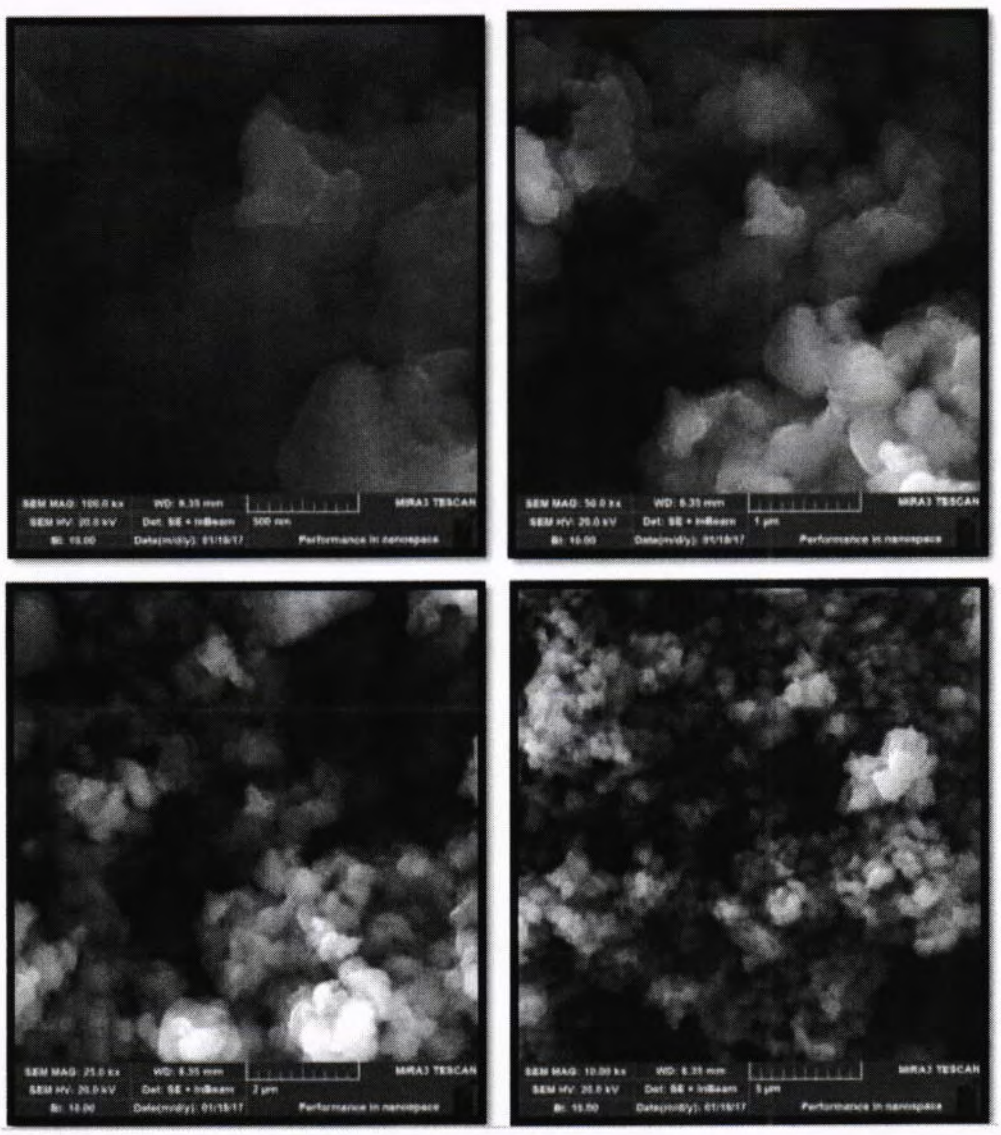

Figure 4.7: Scanning electron microscopic images of iron oxide nanoparticles (prepared by using 25 ml of mint extract) at different magnifications

Figure 4.7 shows the scanning electron microscopic (SEM) images of iron oxide NPs prepared by method 2. These results indicate that by increasing extract quantity, the particle size and shape becomes more difficult and irregular due to agglomeration. It is reported that an increase in the alkalinity of the synthetic system will also effect the phase of product [87].

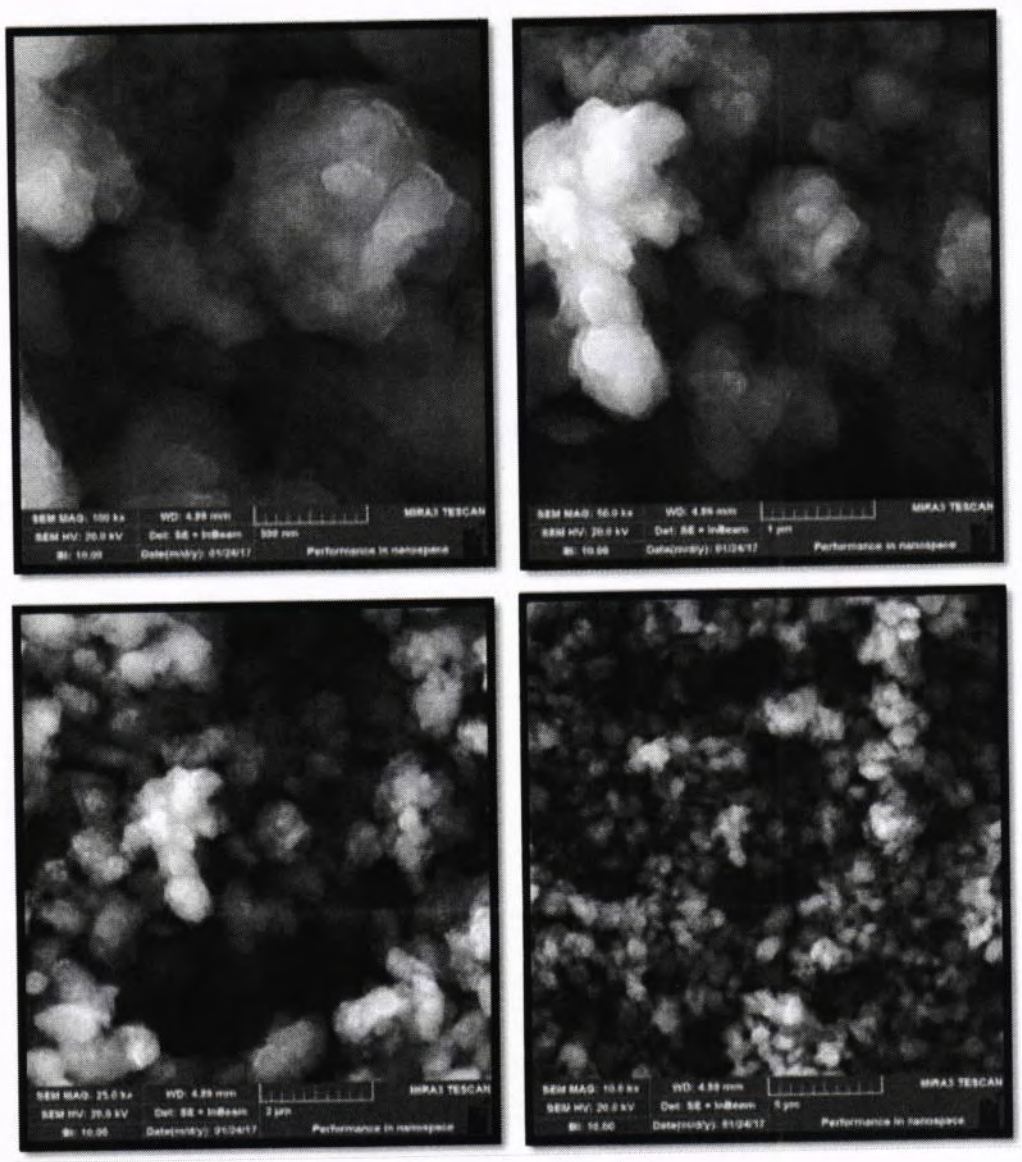

Figure 4.8: Scanning electron microscopic images of iron oxide NPs prepared by using ginger extract

The SEM images of iron oxide nanoparticles that is synthesized by using the extract of ginger, these nanoparticles are encapsulated inside the plant matrixes. Due to agglomeration shape of particles are difficult to examine as shown in figure 4.8.

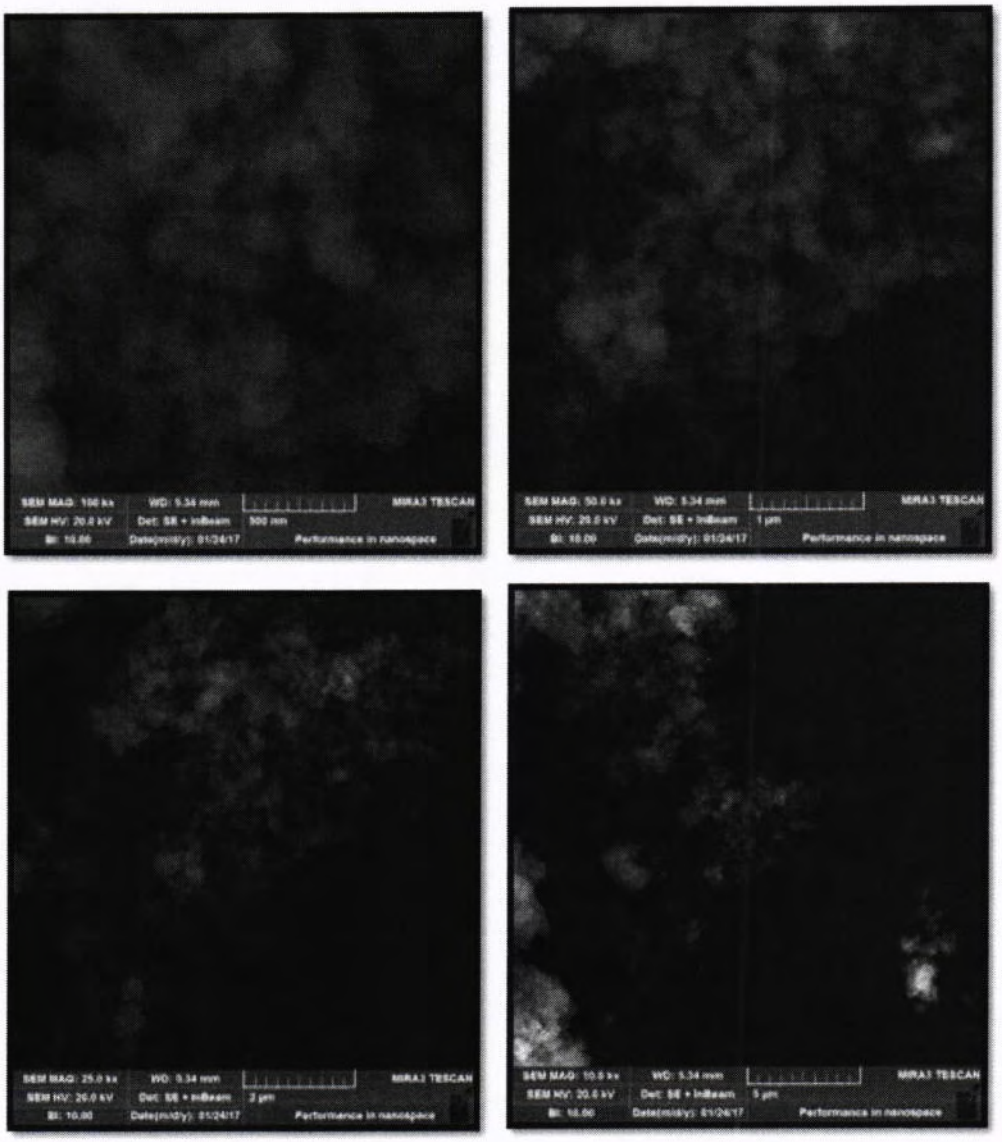

Figure 4.9: SEM images of iron oxide NPs prepared by using spinach leaves extract

Figure 4.9 shows the SEM images of iron oxide nanoparticles prepared by using spinach leaves extract. The size of these particles is also less than 100 nm.

4.4 Compositional investigation via EDX:

The energy dispersive X-ray spectroscopy is used to observe the composition of different elements present in sample.

4.4.1 EDX analysis of iron oxide NPs via Chemical synthesis:

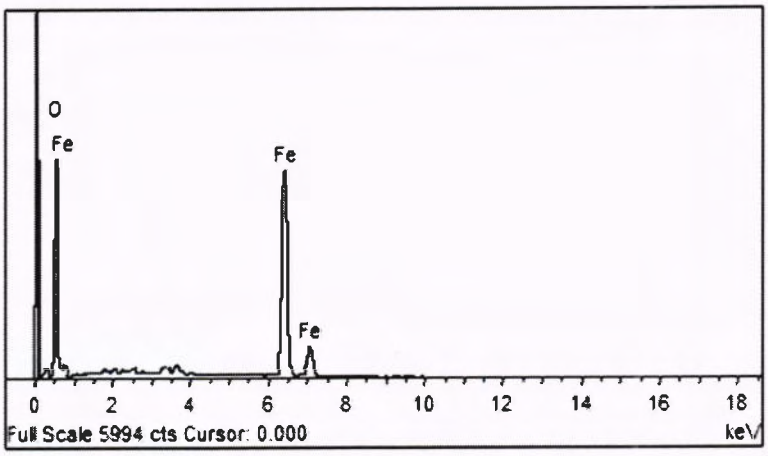

Figure 4.10: EDX spectrum of chemically synthesized Fe_3O_4 nanoparticles

Table 1: Elemental analysis of Fe_3O_4 nanoparticles

Element	Weight %	Atomic %
O k	25.51	54.45
Fe k	74.49	45.55
Total	**100**	**100**

Figure 4.10 shows the EDX graph of Fe_3O_4 nanoparticles. It clearly shows only Fe (iron) and O (oxygen) elements in as-prepared nanoparticles without any impurities. Hence, the EDX analysis reveals that the as synthesized Fe_3O_4 nanoparticles are in perfect stoichiometry [88].

4.4.2 EDX analysis of iron oxide NPs via Green synthesis:

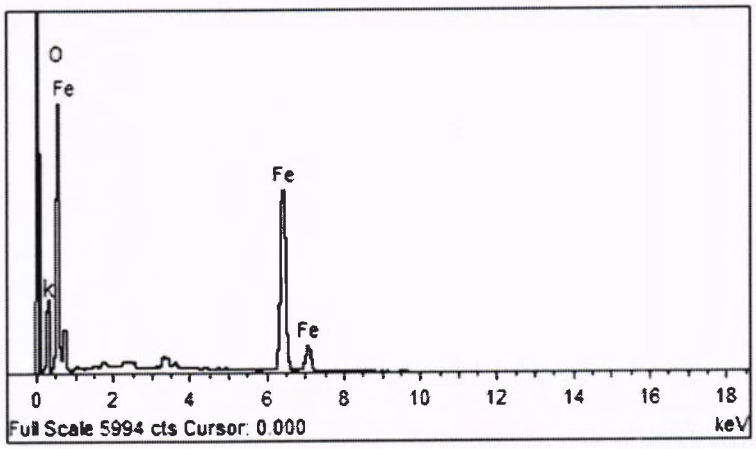

Figure 4.11: EDX spectrum of iron oxide nanoparticles (P_1)

Table 2: Elemental analysis of iron oxide nanoparticles (P_1)

Element	Weight %	Atomic %
O k	30.01	57.61
Fe k	68.97	41.94
K k	1.03	0.45
Total	**100**	**100**

Figure 4.11 describes the EDX spectrum for iron oxide NPs prepared by using mint leaves extract.

It indicates that prepared sample comprises of iron and oxygen, which confirm the formation of iron oxide. The little peak assigned to potassium element came from plant resource. Potassium exists in plants and helps in closing and opening of stomata [89].

It can be clearly seen from Table 2 that the sample mainly comprises of iron (wt % 68.97), oxygen (wt % 30.01) and some potassium (wt% 1.03).

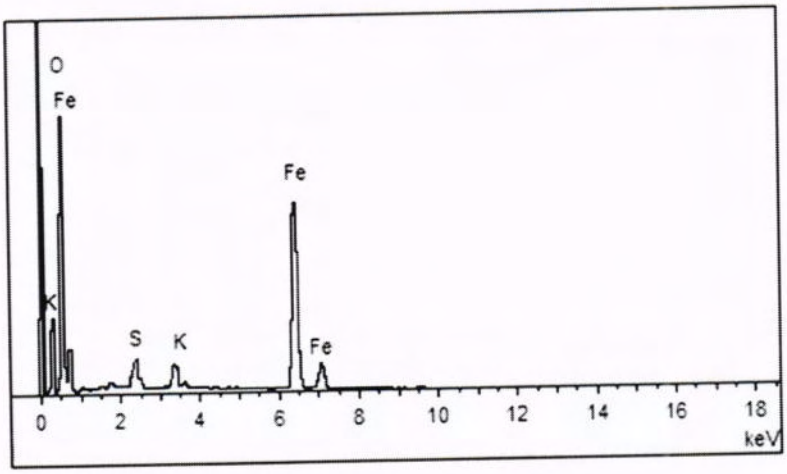

Figure 4.12: EDX spectrum of iron oxide NPs (P_2)

Table 3: Elemental analysis of iron oxide nanoparticles (P_2)

Element	Weight %	Atomic %
O k	38.03	64.59
Fe k	57.09	31.87
S k	1.93	1.53
K k	2.95	2.01
Total	**100**	**100**

Figure 4.12 indicates the EDX spectrum of iron oxide NPs (P_2) prepared by using ginger extract.

The above data clearly demonstrates and confirm the formation of iron oxide. It can be clearly seen from Table 3 that the sample mainly comprises of oxygen (wt% 38.03), iron (wt% 57.09), potassium (wt% 2.95) and some sulphur (wt% 1.93). The peaks assigned to potassium and sulphur came from ginger source.

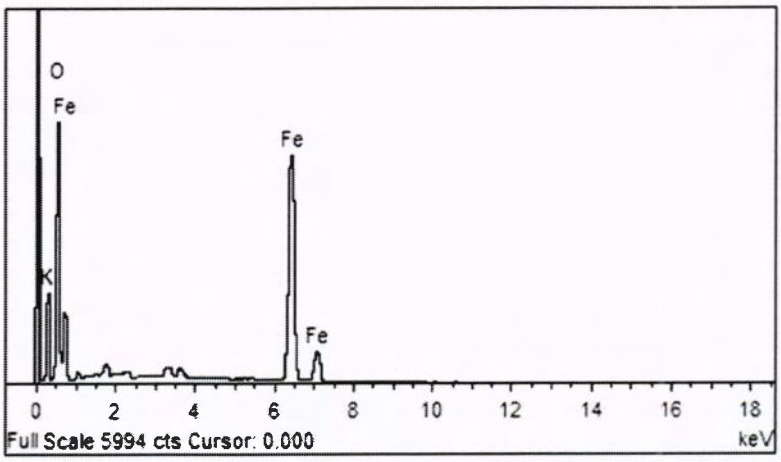

Figure 4.13: EDX spectrum of iron oxide nanoparticles (P_3)

Table 4: Elemental analysis of iron oxide nanoparticles (P_3)

Element	Weight %	Atomic %
O k	34.98	62.35
Fe k	62.37	35.71
K k	2.65	1.94
Total	100	100

Figure 4.13 shows the EDX spectrum of iron oxide nanoparticles synthesized by using spinach extract. It indicates that prepared sample comprises of iron and oxygen. The little peak assigned to potassium element came from plant resource.

It can be clearly seen from Table 4 iron content (wt% 62.37) is more than oxygen content (wt% 34.98).

4.5 Fourier Transform Infrared Spectroscopy:

Fourier Transform Infrared Spectroscopy (FTIR) is used to investigate the chemical bonding variation, impurities, phases and compositions of samples and surface chemistry.

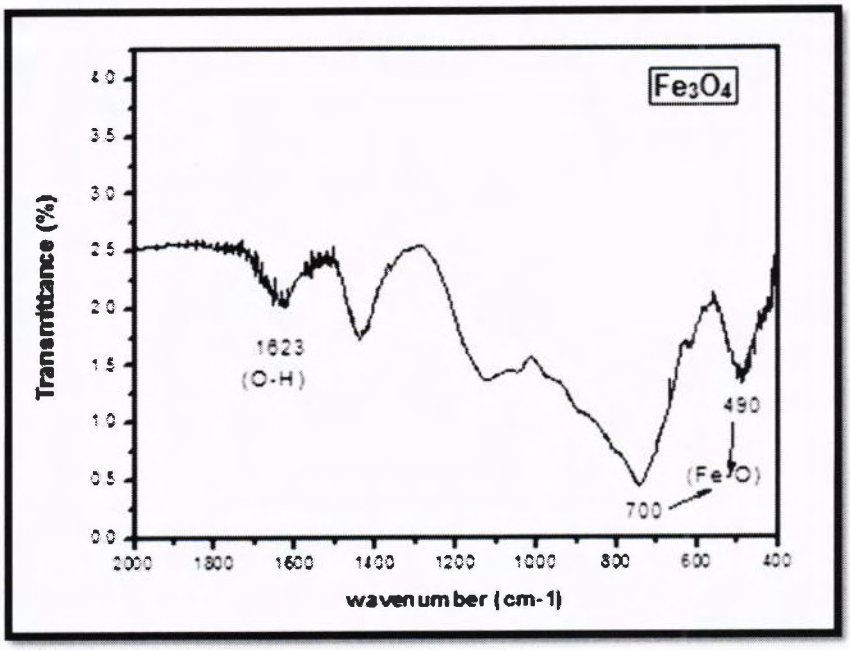

Figure 4.14: FTIR spectrum of magnetite NPs (chemical method)

The bands from 400 to 700 cm^{-1} signifies the lattice vibrations of iron and oxygen bonding, as shown in figure 4.14. This confirm the formation of pure phase of magnetite nanoparticles.

The band at 1623 cm^{-1} corresponds to the absorbed water in material due to O-H stretching vibrations. These results are similar with magnetite NPs investigated previously [90].

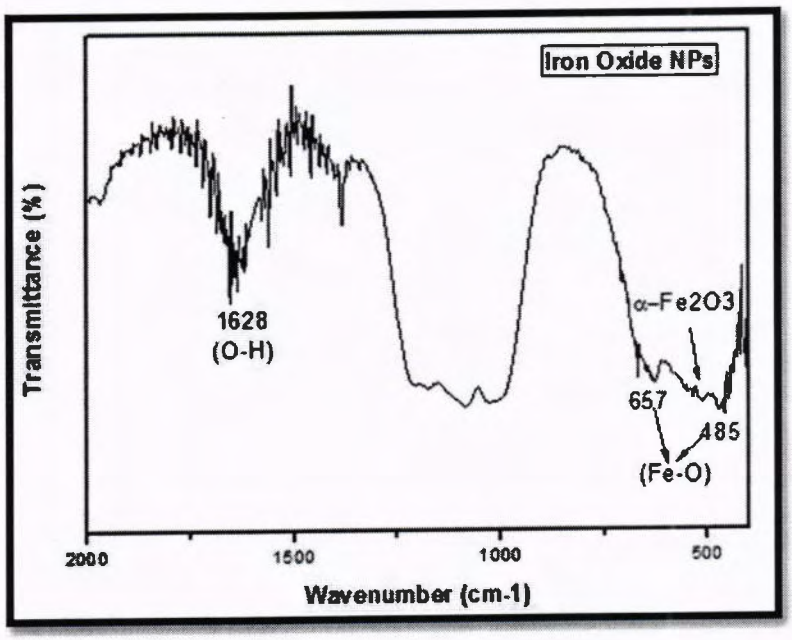

Figure 4.15: FTIR spectrum of iron oxide NPs using 7 ml of mint leaves extract

In figure 4.15, the bands at 485 and 657 cm^{-1} are due to lattice vibrations of iron and oxygen bonding. This confirm the formation of magnetite nanoparticles. The band at 520 cm^{-1} signifies the presence of α-Fe_2O_3 which is also confirmed in XRD analysis. The band at 1628 cm^{-1} corresponds to the absorbed water in material due to O-H stretching vibrations [91].

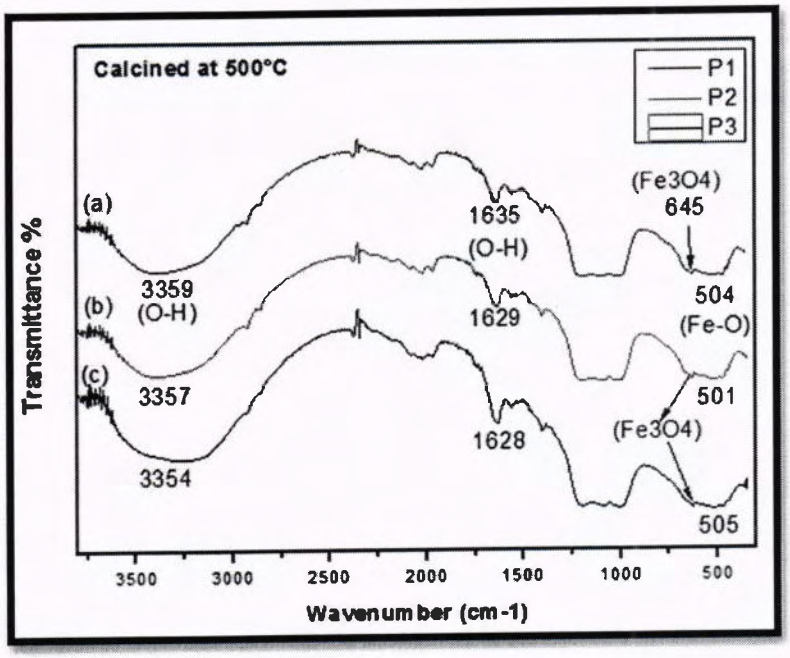

Figure 4.16: FTIR spectrum of iron oxide NPs, comparison of three different plants (mint P_1, ginger P_2, spinach P_3)

The peak at 3359 ,3357, 3354 cm^{-1} in P_1, P_2, P_3 are because of O-H stretching vibrations arises on nanoparticles due to the presence of hydroxyl groups from the water. The absorption peaks at 1635, 1629, 1628 cm^{-1} are also due to the stretching vibrations of O-H groups.

The absorption bands appeared at 504, 501, 505 cm^{-1} which corresponds to Fe–O bond vibration of α-Fe_2O_3 nanoparticles. All these values well-matched with the reported values of Kim et al [92]. The band at 645 cm^{-1} signifies the presence of Fe_3O_4 NPs which is also confirmed in XRD analysis [93].

4.6 Vibrating sample magnetometer analysis:

Magnetic properties of the prepared samples were analysed by vibrating sample magnetometer.

4.6.1 VSM analysis of iron oxide NPs via chemical synthesis:

Magnetic properties of the nanoparticles were observed at room temperature and magnetic field sweeping from -10,000 Oe to 10,000 Oe.

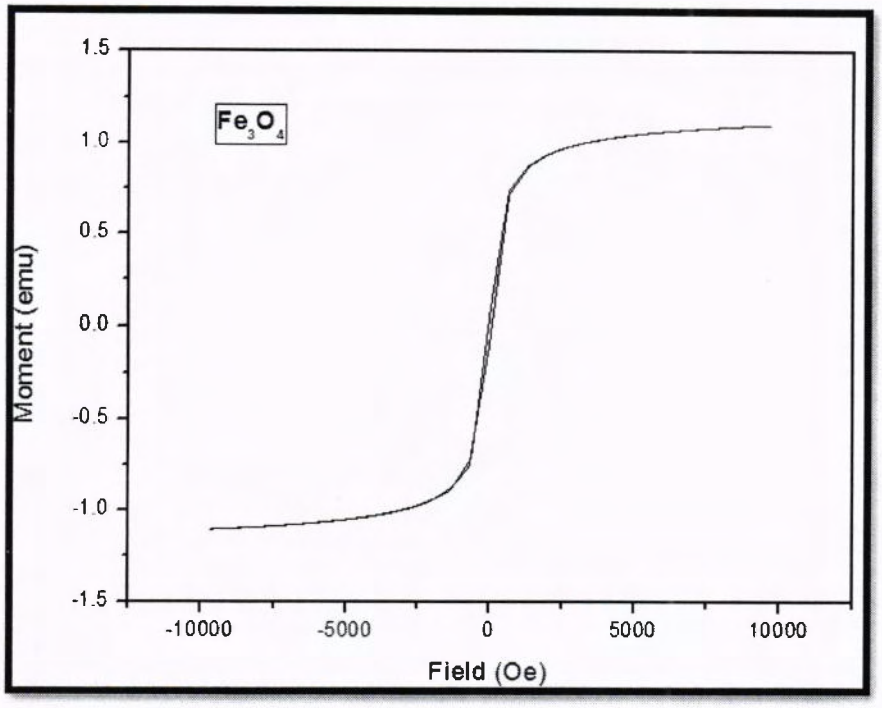

Figure 4.17: Ferromagnetic hysteresis loop of Fe_3O_4 nanoparticles via chemical synthesis

In figure 4.17, a small hysteresis loop is observed which shows that Fe_3O_4 nanoparticles have ferromagnetic behaviour at room temperature and all magnetic spins are fully aligned in the direction of applied field.

The coercivity (H_c) and saturation magnetization values are 59.635 Oe and 1.1034 emu/g respectively.

4.6.2 VSM analysis of iron oxide NPs via green synthesis:

The magnetic properties of green synthesized nanoparticles were observed at room temperature via VSM.

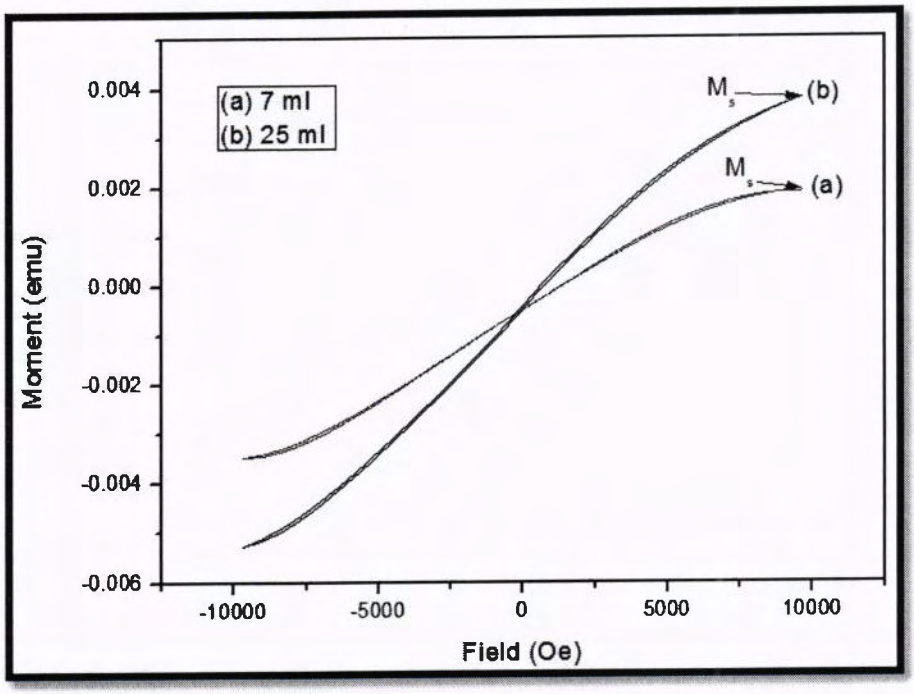

Figure 4.18: Weak ferromagnetic hysteresis loop of IONPs prepared by using **(a)** 7 ml mint extract (M_1), **(b)** 25 ml mint extract (M_2)

Figure 4.18 shows that iron oxide nanoparticles have weak ferromagnetic behaviour at room temperature with low coercivity and remanent magnetization.

The saturation magnetization (M_s) values of M_1 & M_2 are 0.32 and 0.52 emu/g respectively. As seen in figure, the sample prepared with 25 ml of mint leaves extract has higher saturation magnetization (M_s) value.

Figure 4.19 shows the ferromagnetic hysteresis loop of iron oxide nanoparticles prepared by 7 and 25 ml of ginger extract.

The saturation magnetization (Ms) values of M_1 & M_2 are 0.41 and 0.68 emu/g respectively. These results also revealed that the sample prepared by M_2 has higher saturation magnetization.

Hence it is concluded that with the increase of particle size the saturation magnetization also increased [94]. The results obtained from VSM and XRD analysis are in good agreement with each other.

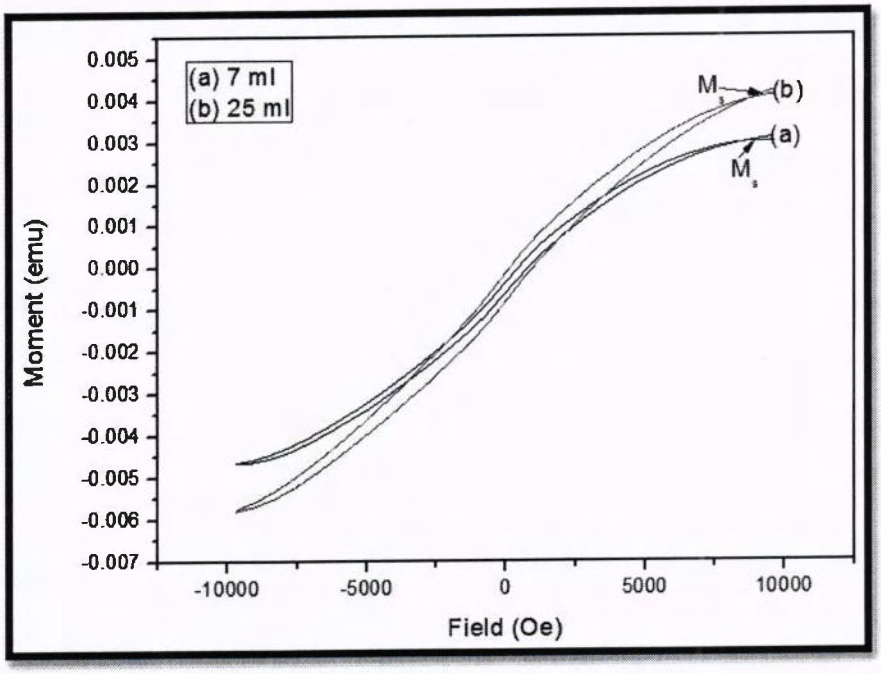

Figure 4.19: Ferromagnetic hysteresis loop of IONPs prepared by using **(a)** 7 ml of ginger extract (M_1), **(b)** 25 ml of ginger extract (M_2)

The nanoparticles obtained via green synthesis showed lower magnetic properties than chemically synthesized nanoparticles.

Conclusions

- Iron oxide nanoparticles are successfully synthesized via chemical and green route.
- In green approach, the extract of ginger, mint and spinach leaves are used, without using any chemical stabilizer and reducing agent.
- X-Ray diffraction study indicated that there are two phases, magnetite is dominating phase at 300 °C and hematite is dominating phase at 500 °C.
- FTIR spectroscopy also confirmed the presence of these two phases.
- The SEM analysis showed that the prepared nanoparticles are less than 100 nm in size and shape is nearly spherical.
- EDX results indicated that prepared samples are comprises of iron and oxygen, which confirms the formation of iron oxide nanoparticle.
- VSM study showed the ferromagnetic behaviour of nanoparticles at room temperature. The increase of saturation magnetization with the increase of particle size was also observed.

References:

1. Geetha, R., Ashokkumar, T., Tamilselvan, S., Govindaraju, K., Sadiq, M. and Singaravelu, G. (2013). Green synthesis of gold nanoparticles and their anticancer activity. *Cancer Nanotechnol*, 4, 91–98.
2. Gupta, A. K., & Gupta, M. (2005). Synthesis and surface engineering of iron oxide nanoparticles for biomedical applications. *Biomaterials*, 26(18), 3995-4021.
3. Jin, R. (2012). The impacts of nanotechnology on catalysis by precious metal nanoparticles. *Nanotechnology Reviews*, 1(1), 31-56.
4. Qu, X., Alvarez, P. J., & Li, Q. (2013). Applications of nanotechnology in water and wastewater treatment. *Water research*, *47*(12), 3931-3946.
5. Shi, J., Zhu, Y., Zhang, X., Baeyens, W. R., & Garcıa-Campana, A. M. (2004). Recent developments in nanomaterial optical sensors. *TrAC Trends in Analytical Chemistry*, *23*(5), 351-360.
6. Frey, N. A., & Sun, S. (2010). Magnetic nanoparticle for information storage applications. *Inorganic Nanoparticles: Synthesis, Application, and Perspective*, 33-68.
7. Jain, P. K., Huang, X., El-Sayed, I. H., & El-Sayed, M. A. (2007). Review of some interesting surface plasmon resonance-enhanced properties of noble metal nanoparticles and their applications to biosystems. *Plasmonics*, *2*(3), 107-118.
8. Cornell, R. M., & Schwertmann, U. (2003). The iron oxides: structure, properties, reactions, occurrences and uses. John Wiley & Sons.
9. Greenwood, Norman N.; Earnshaw, Alan (1997). Chemistry of the Elements (2nd ed.). Butterworth-Heinemann. ISBN 0-08-037941-9.
10. Machala, L., Tuček, J., & Zboril, R. (2011). Polymorphous transformations of nanometric iron (III) oxide: a review. *Chemistry of materials*, *23*(14), 3255-3272.
11. Machala, L., Tuček, J., & Zboril, R. (2011). Polymorphous transformations of nanometric iron (III) oxide: a review. *Chemistry of materials*, *23*(14), 3255-3272.
12. Chirita, M., Grozescu, I., Taubert, L., Radulescu, H., Princz, E., Stefanovits-Bányai, É., ... & Muntean, C. (2009). Fe_2O_3–nanoparticles, physical properties and their photochemical and photoelectrochemical applications. *Chem. Bull*, *54*(68), 1-8.
13. Banerjee, R., Katsenovich, Y., Lagos, L., McIintosh, M., Zhang, X., & Li, C. Z. (2010). Nanomedicine: magnetic nanoparticles and their biomedical applications. *Current medicinal chemistry*, *17*(27), 3120-3141.

14. Ma, M., Zhang, Y., Guo, Z., & Gu, N. (2013). Facile synthesis of ultrathin magnetic iron oxide nanoplates by Schikorr reaction. *Nanoscale research letters*, *8*(1), 16.

15. Spaldin, N. A. (2010). *Magnetic materials: fundamentals and applications*. Cambridge University Press.

16. McNab, T. K., Fox, R. A., & Boyle, A. J. F. (1968). Some magnetic properties of magnetite (Fe_3O_4) microcrystals. *Journal of Applied Physics*, *39*(12), 5703-5711.

17. Buzea, C., Pacheco, I. I., & Robbie, K. (2007). Nanomaterials and nanoparticles: Sources and toxicity. *Biointerphases*, *2*(4), MR17-MR71.

18. Raj, K., Moskowitz, B., & Casciari, R. (1995). Advances in ferrofluid technology. *Journal of magnetism and magnetic materials*, *149*(1-2), 174-180.

19. McMichael, R. D., Shull, R. D., Swartzendruber, L. J., Bennett, L. H., & Watson, R. E. (1992). Magnetocaloric effect in superparamagnets. *Journal of magnetism and magnetic materials*, *111*(1-2), 29-33.

20. McMichael, R. D., Shull, R. D., Swartzendruber, L. J., Bennett, L. H., & Watson, R. E. (1992). Magnetocaloric effect in superparamagnets. *Journal of magnetism and magnetic materials*, *111*(1-2), 29-33.

21. Rahman, M. M., Jamal, A., Khan, S. B., & Faisal, M. (2011). Fabrication of highly sensitive ethanol chemical sensor based on Sm-doped Co_3O_4 nanokernels by a hydrothermal method. *The Journal of Physical Chemistry C*, *115*(19), 9503-9510.

22. Rahman, M. M., Jamal, A., Khan, S. B., & Faisal, M. (2011). CuO codoped ZnO based nanostructured materials for sensitive chemical sensor applications. *ACS applied materials & interfaces*, *3*(4), 1346-1351.

23. Rahman, M. M., Umar, A., & Sawada, K. (2009). Development of amperometric glucose biosensor based on glucose oxidase co-immobilized with multi-walled carbon nanotubes at low potential. *Sensors and Actuators B: Chemical*, *137*(1), 327-333.

24. Garcia, K. E., Morales, A. L., Barrero, C. A., Arroyave, C. E., & Greneche, J. M. (2004). Magnetic and crystal structure refinement in akaganeite nanoparticle. *Physica B: Condensed Matter*, *354*(1), 187-190.

25. Musić, S., Šarić, A., & Popović, S. (1997). Effects of urotropin on the formation of β-FeOOH. *Journal of molecular structure*, 410, 153-156.

26. Brown, A. S. C., Hargreaves, J. S. J., & Rijniersce, B. (1998). A study of the structural and catalytic effects of sulfation on iron oxide catalysts prepared from goethite and ferrihydrite precursors for methane oxidation. *Catalysis letters*, *53*(1), 7-13.

27. Mittal, A. K., Chisti, Y., & Banerjee, U. C. (2013). Synthesis of metallic nanoparticles using plant extracts. *Biotechnology advances*, 31(2), 346-356.

28. Chen, J., Xu, L., Li, W., & Gou, X. (2005). α-Fe_2O_3 nanotubes in gas sensor and lithium-ion battery applications. *Advanced Materials*, 17(5), 582-586.

29. Zeng, H., Li, J., Liu, J. P., Wang, Z. L., & Sun, S. (2002). Exchange-coupled nanocomposite magnets by nanoparticle self-assembly. *Nature*, *420*(6914), 395-398.

30. Gnanaprakash, G., Philip, J., Jayakumar, T., & Raj, B. (2007). Effect of digestion time and alkali addition rate on physical properties of magnetite nanoparticles. *The Journal of Physical Chemistry B*, *111*(28), 7978-7986.

31. Topal, U., & Aksan, M. A. (2016). Phase stabilization of magnetite (Fe_3O_4) nanoparticles with B_2O_3 addition: A significant enhancement on the phase transition temperature. *Journal of Magnetism and Magnetic Materials*, *406*, 123-128.

32. Bayindir, M., Sorin, F., Abouraddy, A. F., Viens, J., Hart, S. D., Joannopoulos, J. D., & Fink, Y. (2004). Metal–insulator–semiconductor optoelectronic fibres. *Nature*, *431*(7010), 826-829.

33. Tartaj, P., Veintemillas-Verdaguer, S., & Serna, C. J. (2003). The preparation of magnetic nanoparticles for applications in biomedicine. *Journal of Physics D: Applied Physics*, *36*(13), R182.

34. Nikiforov, V. N., Koksharov, Y. A., Polyakov, S. N., Malakho, A. P., Volkov, A. V., Moskvina, M. A., ... & Irkhin, V. Y. (2013). Magnetism and Verwey transition in magnetite nanoparticles in thin polymer film. *Journal of Alloys and Compounds*, *569*, 58-61.

35. Bautista, M. C., Bomati-Miguel, O., del Puerto Morales, M., Serna, C. J., & Veintemillas-Verdaguer, S. (2005). Surface characterisation of dextran-coated iron oxide nanoparticles prepared by laser pyrolysis and coprecipitation. *Journal of Magnetism and Magnetic Materials*, 293(1), 20-27.

36. Tang, J., Myers, M., Bosnick, K. A., & Brus, L. E. (2003). Magnetite Fe_3O_4 nanocrystals: spectroscopic observation of aqueous oxidation kinetics. *The Journal of Physical Chemistry B*, *107*(30), 7501-7506.

37. Chamritski, I., & Burns, G. (2005). Infrared-and Raman-active phonons of magnetite, maghemite, and hematite: a computer simulation and spectroscopic study. *The Journal of Physical Chemistry B*, *109*(11), 4965-4968.

38. Dadashi, S., Poursalehi, R., & Delavari, H. (2015). Structural and optical properties of pure iron and iron oxide nanoparticles prepared via pulsed Nd: YAG laser ablation in liquid. *Procedia Materials Science*, 11, 722-726.

39. Martinez, A. I., Garcia-Lobato, M. A., & Perry, D. L. (2009). Study of the properties of iron oxide nanostructures. *Research in Nanotechnology Developments*, *19*, 184-193.

40. Grau-Crespo, R., Al-Baitai, A. Y., Saadoune, I., & De Leeuw, N. H. (2010). Vacancy ordering and electronic structure of γ-Fe_2O_3 (maghemite): a theoretical investigation. *Journal of Physics: Condensed Matter*, 22(25), 255401.

41. Sheng-Nan, S., Chao, W., Zan-Zan, Z., Yang-Long, H., Venkatraman, S. S., & Zhi-Chuan, X. (2014). Magnetic iron oxide nanoparticles: Synthesis and surface coating techniques for biomedical applications. *Chinese Physics B*, 23(3), 037503.

42. Manikandan, A., Vijaya, J. J., Mary, J. A., Kennedy, L. J., & Dinesh, A. (2014). Structural, optical and magnetic properties of Fe_3O_4 nanoparticles prepared by a facile microwave combustion method. *Journal of Industrial and Engineering Chemistry*, 20(4), 2077-2085.

43. Thapa, D., Palkar, V. R., Kurup, M. B., & Malik, S. K. (2004). Properties of magnetite nanoparticles synthesized through a novel chemical route. *Materials letters*, 58(21), 2692-2694.

44. Meisen, U., & Kathrein, H. (1999, January). The influence of particle size, shape and particle size distribution on properties of magnetites for the production of toners. *In NIP & Digital Fabrication Conference* (Vol. 1999, No. 2, pp. 556-560). Society for Imaging Science and Technology.

45. Chirita, M., & Grozescu, I. (2008). Iron oxide nanoparticles and their photoelectrochemical and medical applications a short overview. *Annals of the West University of Timisoara. Physics Series*, 52, 121.

46. Auric, P., Van Dang, N., Bandyopadhyay, A. K., & Zarzycki, J. (1982). Superparamagnetism and ferrimagnetism of the small particles of magnetite in a silicate matrix. *Journal of Non-Crystalline Solids*, 50(1), 97-106.

47. Mamani, J. B., Gamarra, L. F., & Brito, G. E. D. S. (2014). Synthesis and characterization of Fe3O4 nanoparticles with perspectives in biomedical applications. *Materials Research*, 17(3), 542-549.

48. Gupta, A. K., & Gupta, M. (2005). Synthesis and surface engineering of iron oxide nanoparticles for biomedical applications. *Biomaterials*, 26(18), 3995-4021.

49. Teja, A. S., & Koh, P. Y. (2009). Synthesis, properties, and applications of magnetic iron oxide nanoparticles. *Progress in crystal growth and characterization of materials*, 55(1), 22-45.

50. Slavov, L., Abrashev, M. V., Merodiiska, T., Gelev, C., Vandenberghe, R. E., Markova-Deneva, I., & Nedkov, I. (2010). Raman spectroscopy investigation of magnetite nanoparticles in ferrofluids. *Journal of Magnetism and Magnetic Materials*, 322(14), 1904-1911.

51. Bouarab, R., Bennici, S., Mirodatos, C., & Auroux, A. (2014). Hydrogen production from the water-gas shift reaction on iron oxide catalysts. *Journal of Catalysts*, 2014.

52. Bee, A., Massart, R., & Neveu, S. (1995). Synthesis of very fine maghemite particles. *Journal of Magnetism and Magnetic Materials*, 149(1-2), 6-9.

53. Sheng-Nan, S., Chao, W., Zan-Zan, Z., Yang-Long, H., Venkatraman, S. S., & Zhi-Chuan, X. (2014). Magnetic iron oxide nanoparticles: Synthesis and surface coating techniques for biomedical applications. *Chinese Physics B*, 23(3), 037503.

54. Mihir, H., & Siddhivinayak, B. (2015). Calcination and Microwave Assisted Biological Synthesis of Iron Oxide Nanoparticles and Comparative Efficiency Studies for Domestic Wastewater Treatment. *Int. Res. J. Environment Sci*, 4(6), 28-36.

55. Martínez-Cabanas, M., López-García, M., Barriada, J. L., Herrero, R., & de Vicente, M. E. S. (2016). Green synthesis of iron oxide nanoparticles. Development of magnetic hybrid materials for efficient As (V) removal. *Chemical Engineering Journal*, 301, 83-91.

56. Venkateswarlu, S., Kumar, B. N., Prasad, C. H., Venkateswarlu, P., & Jyothi, N. V. V. (2014). Bio-inspired green synthesis of Fe 3 O 4 spherical magnetic nanoparticles using Syzygium cumini seed extract. *Physica B: Condensed Matter*, 449, 67-71.

57. Prasad, C., Gangadhara, S., & Venkateswarlu, P. (2016). Bio-inspired green synthesis of Fe_3O_4 magnetic nanoparticles using watermelon rinds and their catalytic activity. *Applied Nanoscience*, 6(6), 797-802.

58. Karaagac, O., & Kockar, H. (2012). Iron Oxide Nanoparticles Co-Precipitated in Air Environment: Effect of [Fe $^{+ 2} $]/[Fe $^{+ 3} $] Ratio. *IEEE Transactions on Magnetics*, 48(4), 1532-1536.

59. Khalil, M. I. (2015). Co-precipitation in aqueous solution synthesis of magnetite nanoparticles using iron (III) salts as precursors. *Arabian Journal of Chemistry*, 8(2), 279-284.

60. Kumar, B., Smita, K., Cumbal, L., & Debut, A. (2014). Biogenic synthesis of iron oxide nanoparticles for 2-arylbenzimidazole fabrication. *Journal of Saudi Chemical Society*, 18(4), 364-369.

61. Mandal, B. K., & Suzuki, K. T. (2002). Arsenic round the world: a review. *Talanta*, 58(1), 201-235.

62. Osaka, T., Matsunaga, T., Nakanishi, T., Arakaki, A., Niwa, D., & Iida, H. (2006). Synthesis of magnetic nanoparticles and their application to bioassays. *Analytical and bioanalytical chemistry*, 384(3), 593-600.

63. Lee, N., Yoo, D., Ling, D., Cho, M. H., Hyeon, T., & Cheon, J. (2015). Iron oxide based nanoparticles for multimodal imaging and magnetoresponsive therapy. *Chemical reviews*, 115(19), 10637-10689.

64. Sangeetha N. and Kumaraguru A.K. (2015). Antitumor Effects and Characterization of Biosynthesized Iron Oxide Nanoparticles Using Seaweeds of Gulf of Mannar. *International journal of Pharma. Sci.*, 7(2), 469-476.

65. Al-Juhaimi, F., & Ghafoor, K. A. S. H. I. F. (2011). Total phenols and antioxidant activities of leaf and stem extracts from coriander, mint and parsley grown in Saudi Arabia. *Pak J Bot*, 43(4), 2235-7.

66. Runnie, I., Salleh, M. N., Mohamed, S., Head, R. J., & Abeywardena, M. Y. (2004). Vasorelaxation induced by common edible tropical plant extracts in isolated rat aorta and mesenteric vascular bed. *Journal of ethnopharmacology*, 92(2), 311-316.

67. Stanisavljević, D. M., Stojičević, S. S., Đorđević, S. M., Zlatković, B. P., Veličković, D. T., Karabegović, I. T., & Lazić, M. L. (2012). Antioxidant activity, the content of total phenols and flavonoids in the ethanol extracts of Mentha longifolia (L.) Hudson dried by the use of different techniques. *Chemical Industry and Chemical Engineering Quarterly*, 18(3), 411-420.

68. Jolivet, J. P., Chanéac, C., & Tronc, E. (2004). Iron oxide chemistry. From molecular clusters to extended solid networks. *Chemical Communications*, (5), 481-483.

69. Peng, S., Wang, C., Xie, J., & Sun, S. (2006). Synthesis and stabilization of monodisperse Fe nanoparticles. *Journal of the American Chemical Society*, 128(33), 10676-10677.

70. Hinneburg, I., Dorman, H. D., & Hiltunen, R. (2006). Antioxidant activities of extracts from selected culinary herbs and spices. *Food chemistry*, 97(1), 122-129.

71. Prakash, J. (2010). Chemical composition and antioxidant properties of ginger root (Zingiber officinale). *Journal of Medicinal Plants Research*, 4(24), 2674-2679.

72. Ajayi, O. B., Akomolafe, S. F., & Akinyemi, F. T. (2013). Food value of two varieties of ginger (Zingiber officinale) commonly consumed in Nigeria. *ISRN nutrition*, 2013.

73. Iravani, S. (2011). Green synthesis of metal nanoparticles using plants. *Green Chemistry*, 13(10), 2638-2650.

74. Abbas, M., Rao, B. P., Islam, M. N., Naga, S. M., Takahashi, M., & Kim, C. (2014). Highly stable-silica encapsulating magnetite nanoparticles (Fe_3O_4/SiO_2) synthesized using single surfactantless-polyol process. *Ceramics International*, 40(1), 1379-1385.

75. Velmurugan, K., Venkatachalapathy, V. S. K., & Sendhilnathan, S. (2010). Synthesis of nickel zinc iron nanoparticles by coprecipitation technique. *Materials Research*, 13(3), 299-303.

76. Li, Y. S., Church, J. S., & Woodhead, A. L. (2012). Infrared and Raman spectroscopic studies on iron oxide magnetic nano-particles and their surface modifications. *Journal of Magnetism and Magnetic Materials*, 324(8), 1543-1550.

77. Feitknecht, W., & Mannweiler, U. (1967). Der Mechanismus der Umwandlung von γ-zu α-Eisensesquioxid [1]. *Helvetica Chimica Acta*, 50(2), 570-581.

78. Cudennec, Y., & Lecerf, A. (2006). The transformation of ferrihydrite into goethite or hematite, revisited. *Journal of Solid State Chemistry*, 179(3), 716-722.

79. Duvigneaud, P. H., & Derie, R. (1980). Shape effects on crystallite size distributions in synthetic hematites from X-ray line-profile analysis. *Journal of Solid State Chemistry*, 34(3), 323-333.

80. Morales, J., Tirado, J. L., & Macias, M. (1984). Changes in crystallite size and microstrains of hematite derived from the thermal decomposition of synthetic akaganéite. *Journal of Solid State Chemistry*, 53(3), 303-312.

81. Chernyshova, I. V., Hochella Jr, M. F., & Madden, A. S. (2007). Size-dependent structural transformations of hematite nanoparticles. 1. Phase transition. *Physical Chemistry Chemical Physics*, 9(14), 1736-1750.

82. Belin, T., Guigue-Millot, N., Caillot, T., Aymes, D., & Niepce, J. C. (2002). Influence of grain size, oxygen stoichiometry, and synthesis conditions on the γ-Fe_2O_3 vacancies ordering and lattice parameters. *Journal of Solid State Chemistry*, 163(2), 459-465.

83. Mamani, J. B., Gamarra, L. F., & Brito, G. E. D. S. (2014). Synthesis and characterization of Fe_3O_4 nanoparticles with perspectives in biomedical applications. *Materials Research*, 17(3), 542-549.

84. Liu, Y. W., Guan, M. X., Feng, L., Deng, S. L., Bao, J. F., Xie, S. Y., ... & Zheng, L. S. (2012). Facile and straightforward synthesis of superparamagnetic reduced graphene

oxide–Fe_3O_4 hybrid composite by a solvothermal reaction. *Nanotechnology*, 24(2), 025604.

85. Yew, Y. P., Shameli, K., Miyake, M., Kuwano, N., Khairudin, N. B. B. A., Mohamad, S. E. B., & Lee, K. X. (2016). Green synthesis of magnetite (Fe_3O_4) nanoparticles using seaweed (Kappaphycus alvarezii) extract. *Nanoscale research letters*, 11(1), 1-7.
86. Gawande, M. B., Rathi, A. K., Nogueira, I. D., Varma, R. S., & Branco, P. S. (2013). Magnetite-supported sulfonic acid: a retrievable nanocatalyst for the Ritter reaction and multicomponent reactions. *Green Chemistry*, 15(7), 1895-1899.
87. Issa, B., Obaidat, I. M., Albiss, B. A., & Haik, Y. (2013). Magnetic nanoparticles: surface effects and properties related to biomedicine applications. *International journal of molecular sciences*, 14(11), 21266-21305.
88. Chaki, S. H., Malek, T. J., Chaudhary, M. D., Tailor, J. P., & Deshpande, M. P. (2015). Magnetite Fe_3O_4 nanoparticles synthesis by wet chemical reduction and their characterization. *Advances in Natural Sciences: Nanoscience and Nanotechnology*, 6(3), 035009.
89. Talbott, L. D., & Zeiger, E. (1996). Central roles for potassium and sucrose in guard-cell osmoregulation. *Plant Physiology*, 111(4), 1051-1057.
90. Zhang, Y., Kohler, N., & Zhang, M. (2002). Surface modification of superparamagnetic magnetite nanoparticles and their intracellular uptake. *Biomaterials*, 23(7), 1553-1561.
91. Nassar, M. Y., Ahmed, I. S., Mohamed, T. Y., & Khatab, M. (2016). A controlled, template-free, and hydrothermal synthesis route to sphere-like α-Fe_2O_3 nanostructures for textile dye removal. *RSC Advances*, 6(24), 20001-20013.
92. Kim, K. D., Kim, S. S., Choa, Y., & Kim, H. T. (2007). Formation and Surface Modification of Fe_3O_4 Nanoparticles by Co-precipitation and Sol-gel Method. *Journal of Industrial and Engineering Chemistry-SEOUL-*, 13(7), 1137.
93. Sun, J., Zhou, S., Hou, P., Yang, Y., Weng, J., Li, X., & Li, M. (2007). Synthesis and characterization of biocompatible Fe_3O_4 nanoparticles. *Journal of biomedical materials research Part A*, 80(2), 333-341.
94. Zhang, M., Zi, Z., Liu, Q., Zhang, P., Tang, X., Yang, J., ... & Dai, J. (2013). Size effects on magnetic properties of prepared by sol-gel method. *Advances in Materials Science and Engineering*, *2013*.